Brigham Young University

BYU ScholarsArchive

2008-07-17

Differential Expression and Functional Characterization of Alpha3 Beta2 Neuronal Nicotinic Acetylcholine Receptors

John Hideo Mizukawa
Brigham Young University - Provo

Follow this and additional works at: https://scholarsarchive.byu.edu/etd

Part of the Cell and Developmental Biology Commons, and the Physiology Commons

DIFFERENTIAL EXPRESSION AND FUNCTIONAL

CHARACTERIZATION OF ALPHA3 BETA2

NEURONAL NICOTINIC

ACETYLCHOLINE

RECEPTORS

by

John H. Mizukawa II

A thesis submitted to the faculty of

Brigham Young University

in partial fulfillment of the requirements for the degree of

Master of Science

Department of Physiology and Developmental Biology

Brigham Young University

August 2008

BRIGHAM YOUNG UNIVERSITY

GRADUATE COMMITTEE APPROVAL

of a thesis submitted by

John H. Mizukawa II

This thesis has been read by each member of the following graduate committee
and by majority vote has been found to be satisfactory.

_____ _____
Date   Sterling N. Sudweeks, Chair

_____ _____
Date   James P. Porter

_____ _____
Date   Scott C. Steffensen

BRIGHAM YOUNG UNIVERSITY

As chair of the candidate's graduate committee, I have read the thesis of John H. Mizukawa II in its final form and have found that (1) its format, citations, and bibliographical style are consistent and acceptable and fulfill university and department style requirements; (2) its illustrative materials including figures, tables, and charts are in place; and (3) the final manuscript is satisfactory to the graduate committee and is ready for submission to the university library.

_____   _____
Date   Sterling N. Sudweeks
                                         Chair, Graduate Committee

Accepted for the Department

                                         _____
                                         Allan M. Judd

Accepted for the College

                                         _____
                                         Rodney J. Brown
                                         Dean, College of Life Sciences

ABSTRACT

DIFFERENTIAL EXPRESSION AND FUNCTIONAL

CHARACTERIZATION OF ALPHA3 BETA2

NEURONAL NICOTINIC

ACETYLCHOLINE

RECEPTORS

John H. Mizukawa II

Department of Physiology and Developmental Biology

Master of Science

Neuronal nicotinic acetylcholine receptors (nAChRs) are expressed in both the

periperhal and central nervous systems, and are involved in pre-, post-, and non-synaptic

control of neuronal activation. In the brain, these receptors play an important role in a

variety of physiological processes such as cognition, development, learning, and memory

formation. Malfunction of these receptors have been implicated in neurodegenerative

diseases like Alzheimer's disease (AD), schizophrenia, and Parkinson's disease. To date,

17 different nAChR subunits, including $\alpha2$-$\alpha7$ and $\beta2$-$\beta4$, have been cloned that can form

homo- and/or hetero-pentameric ionotropic receptors. The unique combinations of

subunit pentamers manifest in distinct functional receptors. Using single-cell real-time

quantitative RT-PCR, we identified the individual expression rates and co-expression rates of the different nAChR subunits in rat CA1 hippocampal interneurons in efforts to characterize functional receptors involved in learning and memory. The two-way combination of subunits with highest expression in hippocampal interneurons was α3β2. Moreover, this combination was expressed in ratios near 1:3 or 3:1 α3 to β2 respectively. To investigate the functionality of α3β2 receptors in different stoichiometries, we injected human α3 and rat β2 subunit mRNA in 1:3, 1:1, and 3:1 ratios into *Xenopus laevis* oocytes for expression. Two-electrode voltage clamp was then performed with the application of different concentrations of ACh to produce full dose-response curves and channel kinetics data. Distinct α3β2 functional channels were identified from the different expression ratios based on significant differences in channel kinetics (i.e.- peak current rise times, peak current decay times, steady state current in forced desensitization) Dose-response curves produced no significant difference in EC_{50} values in the different expression groups. However, there was a trend to greater agonist sensitivity with increased α3 expression relative to β2. α3β2 receptors were further characterized through forced desensitization of the receptors and generation of IV plots. The findings from this study elucidate the neuronal nAChR subunit combinations that form functional channels in hippocampal interneurons.

ACKNOWLEDGEMENTS

TABLE OF CONTENTS

LIST OF TABLES

LIST OF FIGURES

INTRODUCTION

Acetylcholine (ACh) receptors in the mammalian nervous system have been classified into the muscarinic (mAChR) and nicotinic (nAChR) subtypes based on the ability of the agonists muscarine and nicotine to mimic the effects of ACh as a neurotransmitter. Recently, investigation of nAChRs has sharply increased following preclinical and clinical studies indicating that neuronal nAChRs may have a substantial role in mediating cognition, reward and drug addiction, neuronal development, etc. (Bourin, Ripoll et al. 2003; Gotti and Clementi 2004; Jensen, Frolund et al. 2005; Dani JA 2007). Activation of nAChRs can modulate post synaptic fast excitatory neurotransmission, pre-synaptic release of various neurotransmitters (not exclusively ACh transmission), and nonsynaptic neuronal excitability (Figure 1b) (Gotti, Fornasari et al. 1997; Newhouse, Potter et al. 1997; Jones, Sudweeks et al. 1999; Dani JA 2007).

There are three major cholinergic systems in the brain that innervate practically all neural areas. One of these cholinergic systems originates in basal forebrain nuclei and project into the cortex and hippocampus, effectively influencing cognitive functions like learning, memory, attention, etc. Another major cholinergic subsystem originates from neurons in the pedunculopontine tegmentum and the laterodorsal pontine tegmentum, and innervates the thalamus, midbrain, caudal pons, and brain stem. The third cholinergic system arises from striatal interneurons providing innervation to the striatum and olfactory tubercle.(Bourin, Ripoll et al. 2003; Dani JA 2007). The effects of activation of these three pathways can be quite extensive on many distinct brain functions.

Nicotinic acetylcholine receptors (nAChRs) are members of a large, structurally homologous ligand-gated ion channel superfamily together with $GABA_A$, glycine, and 5-

1

HT$_3$ serotonin receptors (Ortells 1995; Jensen, Frolund et al. 2005; Dani JA 2007). Located in a variety of tissues, nAChRs play a functional role in the autonomic nervous system, neuromuscular junction, and brain in vertebrates (Lopez-Hernandez, Sanchez-Padilla et al. 2004; Pimlott and Wyper. 2004; Dani JA 2007). Like every member of the ligand-gated ion channel family, the nAChR is a transmembrane receptor protein consisting of five polypeptide subunits arranged around a "pseudo-axis of symmetry" (Bourin, Ripoll et al. 2003). Each subunit has a large extracellular N-terminal segment, four transmembrane domains, and a small extracellular C-terminal tail (Changeux, Bertrand et al. 1998). The second transmembrane region of each subunit lines the non-specific cation pore and is highly conserved between subunits (Jensen, Frolund et al. 2005). The same subunits also share high homology between species (over 80% conserved amino acid sequences between vertebrate species) (Changeux and Edelstein 2005). The ACh binding site is at the interface between two subunits (one alpha and one beta, with the exception of α7 homomeric channels) in the N-terminal extracellular region (Figures 1a and 2). nAChRs also contain a rather large intracellular amino acid loop between the third and fourth transmembrane regions (Figure 1a Right). This loop is susceptible to modification by intracellular second messenger cascades.

To date, seventeen nAChR subunits have been cloned and identified (α1-10, β1-4, γ, δ, and ε) (Curtis L. 2002; Jensen, Frolund et al. 2005; Gotti, Zoli et al. 2006; Dani JA 2007). The neuronal nAChR subunits include α2-10 and β2-4, of which the majority have been identified to be natively expressed in the central (CNS) and peripheral (PNS) nervous systems (the α8 subunit has only been found in chickens; the α9 and α10 subunits show limited expression in the cochlea) (Jensen, Frolund et al. 2005; Dani JA

2

2007). The physiological, biophysical, and pharmacological properties of nAChRs in the brain are determined by the pentameric co-assembly of these different subunits. Activation of different subtypes of nAChRs (due to unique pentameric assemblages) can differentially modulate, not only neurotransmitter release and synaptic plasticity, but also calcium-dependent cellular events that include activation and modulation of other ion channels, excitability, secretion, motility and migration, gene expression, and cell differentiation and survival (Sher, Chen et al. 2004). These effects can be caused by distinct properties of calcium conductance through different nAChRs. For example, it has been demonstrated that the expression of the α5 subunit in α3β2 and α3β4 containing receptors causes an increase in Ca^{++} permeability (Yu and Role 1998).

Although many subunit combinations have been identified in the CNS, the most commonly investigated mammalian neuronal nAChRs contain the α7 or α4β2 subunits which form homomeric or heteromeric complexes, respectively (Changeux, Bertrand et al. 1998). It is primarily asserted that the majority of brain nAChRs with a high affinity for agonist contain the α4 and β2 subunits, whereas α3 and β4 subunit-containing nAChRs are highly expressed in the peripheral nervous system (Jensen, Frolund et al. 2005). It is also commonly believed that the α4β2 and α3β4 receptor subtypes are natively expressed in a stoichiometric ratio of two α subunits to three β subunits arranged in the specific sequence of αβαββ (Anand R 1991; Boorman, Groot-Kormelink et al. 2000; Jensen, Frolund et al. 2005). However, recent studies have shown that different stoichiometric expressions of the α:β subunit ratio will result in distinct receptor properties (i.e., affinity for agonists/antagonists, current kinetics, etc.). They have also shown that a different stoichiometric expression of the α4β2 receptor subtype can be

forced to deviate from the 2α:3β expression ratio simply by changing the subunit

transfection ratios (Zwart and Vijverberg 1998; Nelson, Kuryatov et al. 2003; Lopez-

Hernandez, Sanchez-Padilla et al. 2004).

The involvement of brain nAChRs in a variety of cognitive and behavioral

systems is sufficiently supported by nAChR knockout studies, which imply that nAChRs

are involved with neurodegenerative disorders including Alzheimers disease (AD),

schizophrenia, epilepsy, autism, and in aging (Figure 3) (Jones, Sudweeks et al. 1999;

Court 2001; Woodruff-Pak DS 2002; Bourin, Ripoll et al. 2003; Dani JA 2007).

Revealed by behavioral and electrophysiological studies, evidence implicates the

nicotinic system is linked in AD and the α7 receptor subtypes are essentially presynaptic,

while the α4/β2 receptor subtypes are pre- and postsynaptic (Gotti, Fornasari et al. 1997).

AD is characterized by accumulation of senile plaques, mainly composed of the beta-

amyloid peptide (Aβ). Even though the exact causes of AD are unknown, different

pathogenesis hypotheses implicating nAChRs made up of α7 subunits have been

proposed, with the receptors exerting a direct or indirect action on the mechanism of Aβ

toxicity. The application of Aβ has recently been shown to impede nAChR function in

rat hippocampal neurons (Pettit, Shao et al. 2001).

Since hippocampal interneurons express various functional combinations of

nAChR subtypes (Jones and Yakel 1997; Frazier, Rollins et al. 1998; Ji 2000; Sudweeks

and Yakel 2000) drugs might be designed to interact selectively with a specific nAChR

subtype and therefore provide different therapeutic opportunities. Thus, drug treatment

may contribute to specific physiological and behavioral functions without causing

adverse or undesired side effects due to interactions with other nAChR subtypes located

4

elsewhere in the nervous system (Levin 2002). In order to fully understand the biophysical and pharmacological properties of functional nAChRs in the brain, we need to identify the underlying subunit combinations expressed in different areas of the brain.

Co-expression of nAChR subunits into non-native cell lines is a technique that is commonly used to facilitate the characterization of nAChR function. Successful heterologous expression of nAChRs has been achieved using human embryonic kidney- (HEK-) 293 cells and *Xenopus laevis* oocytes. For example, several studies examining the function of heterologously expressed nAChRs in the *Xenopus* cell system reveal a diverse pharmacological profile in receptors containing monomeric combinations of α7 (Khiroug, Harkness et al. 2002), and dimer combinations of α2, α3, α4, or α7 in combination with β2 or β4 (Vibat 1995; Elliott, Ellis et al. 1996; Fenster 1997; Khiroug, Harkness et al. 2002). *Xenopus laevis* oocytes also showed no nicotinic response to acetylcholine application unless injected with exogenous nAChR subunit mRNA (Deneris, Boulter et al. 1989). For these studies we injected *Xenopus laevis* oocytes with nAChR subunit mRNA to study the functional properties of α3β2 neuronal nAChRs. The subunit mRNA ratios we used were based on those identified in native rat hippocampal interneurons using quantitative single-cell RT-PCR. Our results provide a characterization of how expression of these two subunits in different ratios can form distinct subtypes of functional ion channels.

MATERIALS AND METHODS

Slice Preparation

The PCR related protocol was followed as described in Burgon 2006. To obtain the interneurons, coronal brain slices (either 300 or 350 μm thick) were made from 8 to 23 day-old Wistar rats using a Vibratome 1000-Plus (Pelco, Redding, CA). The slices were cut in ice-cold oxygenated (95% O_2, 5% CO_2) artificial cerebro-spinal fluid (ACSF in mM: 124 NaCl, 2 KCl, 1 Na H_2PO_4, 26 $NaHCO_3$, 11 Glucose, 2 $CaCl_2$, 1 $MgSO_4$) and placed in room-temperature oxygenated ACSF for at least 30 minutes prior to placing in microscope recording chamber.

Individual hippocampal interneurons from the CA1 *stratum oriens* and *stratum radiatum* (Figure 4) were visually identified using an upright microscope with infrared light, and aspirated into a standard whole-cell patch-clamp pipette (Borosilicate capillaries, Harvard Apparatus, Kent, England) containing 5 μL Intracellular Fluid (ICF in mM: 10 $MgCl_2$, 0.1 $CaCl_2$, 1 EGTA, 10 HEPES, 135 K-Gluconate, Na-2 ATP).

Electrophysiology of Wistar Rat CA1 Hippocampal Interneurons

A whole-cell patch clamp of the interneuron was obtained in voltage-clamp mode prior to cytoplasm aspiration. Interneuron membrane potentials were held at -70 mV.

Primers and Probes

Primers and probes were purchased from Invitrogen (Carlsbad CA). The primers and probes were designed using either Vector NTI version 7.0 (Invitrogen) or Primer Express version 2.0 (ABI Prism, Foster City CA) software.

6

RT Reaction

A cDNA library representing each interneuron was made by running a reverse transcription reaction using BIORAD (Hercules CA) iScript cDNA Synthesis Kit with a final volume of 10 µL.

Multplex Reaction and Real-time Quantitative PCR

A multiplex PCR reaction was run (15 cycles) for each aspirated interneuron using all neuronal nAChR primers as well as primers for 18s rRNA with a final volume of 75 µl. The multiplex reaction was run using reagents by Invitrogen including Platinum® *Taq* DNA Polymerase and PCR nucleotides (10 mM). A second round of PCR was run (60 cycles) for each specific target (18s, α2-α7, and β2-β4) using an ABI 7000 Sequence Detection System (Applied Biosystems, Foster City, CA) utilizing BIORAD iTaq Supermix with ROX. Cycle threshold values for each target were compared to the reference gene 18s for analysis (more in *Real-Time Analysis*).

Standard curves (efficiency tests) for each cDNA target were developed by running 60-cycle real-time quantitative PCR assays on positive controls (rat whole-brain homogenate) for six known concentrations (100, 33.3, 10, 3.33, 1, 0.333 ng cDNA/µL). Upstream (primer +) and downstream (primer -) primer concentrations were adjusted to optimize amplification as reported previously. The efficiency of the amplification reaction is calculated using the slope of the log(concentration) vs. CT plot. The formula for PCR efficiency $= 10^{(-1/\text{slope})} - 1$. Reaction efficiencies were run in triplicate and the amplification efficiencies were compared using ANOVA to determine if there were significant differences between any of the primer/probe sets (18s, α2-α7, and β2-β4).

Real-Time Analysis

After running the real-time quantitative PCR on hippocampal interneurons, raw fluorescence (Delta Rn) values across 60 cycles were curve-fit using a Boltzmann Sigmoidal function with an output of either 2000 or 4000 data points in the new curve using Prism ver. 4.03 (GraphPad Software, San Diego CA). The second derivative graph for the curve-fit data was then determined, also using the GraphPad software. The cycle threshold (CT) value used for quantitative analysis was determined by finding the cycle number (along the x-axis) corresponding to the maximum Delta Rn value (along the y-axis), as described previously (Burgon 2006).

Primer Efficiencies Analysis

Triplicate reactions of each cDNA target were averaged and a linear regression equation was calculated (SLOPE function, Microsoft Excel, Microsoft Office 2003, Redmond WA) of the CT values corresponding to the six known concentrations (100, 33.3, 10, 3.33, 1, 0.333 ng cDNA/µL) in the standard curve primer efficiency tests. The PCR efficiency was then determined by incorporating the slope of the linear equation using the formula described above (see *Multiplex Reaction and Real-Time Quantitative PCR*).

Analysis of mRNA Expression in Rat Hippocampal Interneurons

For comparison between cDNA targets, fold expression values from the triplicate CT averages were calculated as reported previously, but compared to the CT value corresponding to the lowest level of cDNA detection (Livak and Schmittgen 2001). Significance between relative levels of mRNA expression was calculated by comparing

8

mean fold expression values using a Mann-Whitney test (calculated using InStat ver. 3.05, GraphPad software, San Diego CA).

Plasmid DNA Preparation

The human α3 subunit and rat β2 genes were inserted into the pCMV6-XL4 (Origene Technologies, Rockville MD) and the pcDNA 3.1 (Invitrogen, Carlsbad CA) plasmids, respectively, using a digestion and ligation protocol from New England Biolabs (Ipswich MA) and Bioline (London UK), respectively. All plasmids were grown up using a transformation protocol by Yeastern Biotech (Taipei TW) and carried out in accordance with its guidelines. A plasmid isolation and purification protocol was followed using the HiSpeed® plasmid purification kit by QIAGEN Inc. (Valencia CA).

Xenopus Oocyte Isolation

Female *Xenopus laevis* frogs were provided by the National Institute of 30 minutes until notably unresponsive. They were then anesthetized by immersion in a solution containing 0.1% ethylmetaaminobenzoate (MS-222; Sigma) for 20 minutes. The frogs were sacrificed in accordance with guidelines approved by the NIEHS Animal Care and Use Committee by severing the spinal cord. Oocytes were dissected and defolliculated by treatment with collagenase B (Roche Diagnostics, Basel Switzerland, 2 mg/mL) and trypsin inhibitor (GIBCO, Invitrogen, Carlsbad CA, 1 mg/mL) in an calcium-free OR-2 solution [Ca^{2+}-free OR-2 in mM: 82.5 NaCl, 2 KCl, 1 $MgCl_2[6H_2O]$, 5 HEPES (pH 7.5-7.6)] for 2 hours. The cells were then rinsed in a BSA-enriched Ca^{2+}-free OR-2 solution (*same as above* with 1mg/mL BSA). The oocytes were incubated at 18°C gently rotating at roughly 100 rpm in an OR-2 solution containing Ca^{2+} [OR-2 with

Ca^{2+} in mM: 82.5 NaCl, 2.5 KCl, 1.0 Na_2HPO_4, 3.009 NaOH, 5 HEPES, 1.0 $CaCl_2$, 1.0 $MgCl_2$, 2.5 Pyruvic Acid, 0.05 mg/mL Gentamycin Sulfate (pH 7.5-7.6)].

RNA Preparation and Expression in Oocytes

Plasmid DNA containing genes for the human α3 and rat β2 nAChR subunits were linearized by restriction digest using XhoI and NotI, respectively (New England BioLabs). mRNA was then transcribed and capped on the 5' end using the mMessage Machine kit (Ambion, ABI, Foster City CA) according to the protocol provided by the manufacturer. Each oocyte was injected with a total of 20 ng of mRNA (5 ng of α3: 15 ng β2 for the 1:3 expression, 10 ng of α3:10 ng β2 for the 1:1 expression, and 15 ng α3: 5 ng β2 for the 3:1 expression) in a total volume of 50 nL. Injection of 50 nL allowed for visual confirmation of a successful injection. Recordings were performed 2-5 days post-injection.

Electrophysiological Recordings

Current recordings were obtained by performing two-electrode voltage-clamp (Figure 5) on the mRNA injected oocytes with a Geneclamp 500 and pCLAMP 8 software (Axon Instruments, Molecular Devices, Sunnyvale CA). Traces were filtered at 2 kHz and sampled at 5 kHz with a holding potential of -60 mV. Electrodes containing 3 M KCl were formed from borosilicate glass capillaries (Harvard Apparatus, Kent, England) and had resistances of less than 1 MΩ. ACh solutions (1 μM, 10 μM, 100 μM, 300 μM, 1mM, 10 mM, 30 mM) were freshly prepared from a frozen stock solution or powder diluted in an ECF-like bath solution containing 96 mM NaCl, 2 mM KCl, 1.8 mM $CaCl_2$, 1 mM $MgCl_2$, and 5 mM HEPES (pH 7.4). Four different concentrations of

10

ACh were placed into four separate tubes feeding into the same synthetic quartz application pin (0.7 mm id) operated by a computer-controlled valve.

Dose-Response Recordings

Currents elicited from different concentrations of ACh determined that 10 mM ACh resulted in a maximal peak current. A recovery period of 2 minutes following a 1 second 30 mM ACh application was required for current to return to baseline with the flow rate of bath solution replacement approximately 3 mL/min. Therefore, ACh was applied every 2 minutes and allowed to completely wash away before the subsequent application. Because there were only four tubes available for application of different ACh concentrations, the current elicited from 3 different doses of acetylcholine were compared to the maximal response of a 1s 10mM application on that same cell. All currents from every dose of ACh were normalized to the peak current from the 10 mM ACh application (Figure 7).

IV Plots and Forced Desensitization

IV plots were obtained by measuring the maximum current elicited from a 1s 10 mM application of ACh at six holding potentials from -60 to +40 mV (-60 mV, -40 mV, -20 mV, 0 mV, 20 mV, and 40 mV) (Figure 8). ACh application occurred in 2 minute intervals as described above. Forced desensitization curves were produced by continuously applying 300 µM ACh for 55 seconds (Figure 10).

Data Analysis

Peak currents, 10-90% rise times, 90-10% decay times, curve fitting, and Tau calculations were measured and analyzed using Clampfit (Axon Instruments) and Microsoft Excel (Microsoft Office 2003, Redmond WA). Tests of significance using a

two-tailed t-test were also performed in Microsoft Excel. Only P values less than 0.05

were considered significant. GraphPad 4.0 (GraphPad software, Prism) was used to

graph the dose-response curves and calculate the EC_{50}'s from each curve. IV plots were

graphed and curve fitted using Microsoft Excel. Reversal Potentials for the receptors

were calculated by solving the best curve fit equation for y=0 (Figure 9).

RESULTS

Neuronal nAChR Subunit mRNA expression in rat CA1 hippocampal interneurons

Rat CA1 hippocampal interneurons from the *stratum radiatum* and *stratum oriens* were individually aspirated and analyzed for their level of expression of the α2-α10 and β2-β4 neuronal nAChR subunits compared to 18s rRNA expression. Of the 89 interneurons analyzed, 88.8% (n=79) expressed the mRNA of at least one nAChR subunit. In the 79 cells that expressed nAChR subunits, the two-way combination of nAChR subunits with the highest co-expression rate was found to be α3β2 (43.0%, n=34). By excluding two-way combinations of subunits that could not make functional channels (i.e.- α subunits paired with α subunits, β subunits paired with β subunits, α5 with any other subunit, and β3 with any other subunit) the co-expression rates of the remaining subunits decreased as follows: 38% α7β2, 33% α3β4, 27% α4β2, 24% α2β2, 22% α7β4, 20% α2β4, 15% α4β4 (Figure 6).

The α3 subunit was expressed in 59.5% (n=47) of the 79 nAChR expressing interneurons. Coincidentally, the individual β2 subunit expression rate was also 59.5% (n=47). The product of these individual expression rates gives us an expected co-expression rate of 35.4%, which is ~7.6% lower than the 43.0% co-expression we observed. Interestingly, of the 47 cells that expressed the α3 subunit, 72.3% (n=34) also expressed the β2 subunit. Likewise, of the 47 cells that expressed the β2 subunit, 72.3% (n=34) also expressed the α3 subunit. This as well suggests the propensity for α3 and β2 subunits to co-express in CA1 hippocampal interneurons. Furthermore, while unique subunit combinations were found in 47.2% (n=42) of the hippocampal interneurons sampled, the most common single cell combinations were found to both contain α3 and

β2 subunits (**α3**α4α5α7**β2** and **α3**α5**β2**β3β4 were expressed in 4 cells each). The relative fold expression of α3 compared to β2 (and vice versa) in individual interneurons was calculated in order to hypothesize the stoichiometric expression ratio of the α3 and β2 subunits. The α3 subunit demonstrated a 2.5 fold expression over β2 in cells where the α3 subunit was expressed more than the β2 subunit (n=15). In cells that expressed more β2 than α3, the β2 subunit showed a 3.3 fold expression over α3 (n=19). These data convinced us that the α3β2 nAChR subunit combination should be investigated in a 1:3 or 3:1 expression ratio in order to best mimic our observations in native rat CA1 hippocampal interneurons.

10%-90% Rise Times

Two-electrode voltage clamp was performed on *Xenopus laevis* oocytes injected with α3 and β2 subunit mRNA in 1:3, 1:1, and 3:1 ratios in the presence of the agonist ACh. The time required for the current to rise from 10% to 90% of the maximum current elicited from a 1s application of 10 mM ACh was calculated in Clampfit version 9.2 (Molecular Devices, Sunnyvale CA) and potential statistical significance was analyzed in Microsoft Excel (Microsoft Office 2003, Redmond WA). Cells injected with α3 and β2 mRNA in a 1:3 ratio demonstrated an average 10-90% rise time of 221.76 ms ± 47.79. The oocytes injected with α3 and β2 mRNA in a 1:1 and 3:1 ratio produced faster average 10-90% rise times of 143.95 ms ± 30.27, and 98.14 ms ± 9.52, respectively. A two-tailed t-test performed for the two groups of physiological pertinence [the 1:3 (n=40) and 3:1 (n=43) expression groups] revealed a significant difference in 10-90% rise times (P =0.010) (Tables 1a & b, Figure 12). ANOVA was also performed (InStat, GraphPad Software) on the three different expression groups. We found no significant difference of

10-90% rise times between the 1:3 and 1:1 expression groups, nor between the 3:1 and 1:1 expression groups. ANOVA did confirm the significant difference between the 1:3 and 3:1 expression groups. ANOVA failed to demonstrate any significant differences in comparisons involving the 1:1 expression group for any of the parameters tested. Therefore, a two-tailed t-test was performed to indicate significant differences between the 1:3 and the 3:1 expression groups for all parameters tested, since these were the two groups of physiological relevance.

Reversal Potentials

IV plots were produced for each of the expression groups (1:3, 1:1, and 3:1 $\alpha3\beta2$) by measuring the peak current elicited from a 1s application of 10 mM ACh at each of six holding potentials (-60 mV, -40 mV, -20 mV, 0 mV, 20 mV, 40 mV). The IV plots for $\alpha3\beta2$ nAChRs showed considerable inward current rectification (see Figure 8 for example of IV plot). Best fit curves ($R^2 > 0.999$) for the IV plots were calculated in Microsoft Excel and the curve fit equations were solved (y=0) to find the reversal potentials. The cells injected with $\alpha3\beta2$ mRNA in a 1:3 ratio (n=3) showed Nernst potentials averaging -24.65 mV $\pm$ 3.63, while the 1:1 expression group (n=4) and the 3:1 expression group (n=5) produced reversal potentials of -17.58 mV $\pm$ 1.34 and -16.91 mV $\pm$ 1.99, respectively. A two-tailed t-test performed for the two groups of physiological pertinence (1:3 and 3:1 expression groups) showed no significant difference between their reversal potentials (P=0.0845) (Tables 2a & b, Figure 13).

Steady State Current Compared to Peak Current with Extended Agonist Application (Forced Desensitization)

During the forced desensitization of the $\alpha3\beta2$ nAChRs due to a 55s application of 300 μM ACh, we observed a steady state current above the resting baseline (see Figure 9

15

for example). Such a prolonged application and high concentration of ACh would typically evoke a classical agonist-bound desensitized state of the receptor (Giniatullin, Nistri et al. 2005; Gay and Yakel 2007), but we see a low, persistent, steady-state current during the end of the 55s application. The steady-state current at 55 seconds was measured from baseline, calculated into a percent of the peak current, and compared between the different expression groups (1:3, 1:1, 3:1). The average steady-state current during forced desensitization for cells injected with α3 and β2 mRNA in a 1:3 ratio (n=2) was 37.39% ± 0.02 of the initial peak current. The 1:1 expression group (n=4) shared a similar high steady-state current at 41.41% ± 0.09 of the peak current. The 3:1 expression group (n=6) showed a much lower average steady-state current in forced desensitization at 25.29% ± 0.03. A two-tailed t-test on the means of the steady-state currents in the 1:3 and 3:1 expression groups showed that they are significantly different (P=0.0347) (Tables 3a & b, Figure 14).

# of Exponents Used in Curve Fit

The decay curve in forced desensitization showed a slightly irregular pattern, especially at ~7s after the peak (Figure 10). The rebound effect after the 55s application was similar to that seen in human α3β2 currents referenced by Jensen et al. (Jensen, Frolund et al. 2005). Analysis of the decay curve from the peak to the steady state current (excluding the rebound effect at 55s) in forced desensitization was performed in Clampfit to form a best fit curve. The lowest number of exponents used to fit the decay curve with the highest correlation (R^2) was compared between the 1:3, 1:1, and 3:1 α3β2 expression groups. The average number of exponents used to best fit the forced desensitization decay curve in the 1:3 expression group (n=2) was 1.33 ± 0.33. In the 3:1

16

expression group (n=6), the average number of exponents used to fit the forced

desensitization curve was 3.33 ± 0.80. A two-tailed t-test showed no significant

difference between the two groups (P=0.138). The 1:1 expression group (n=4) required

an average of 2.5 exponents ± 0.87 (Tables 4a & b, Figure 15).

90%-10% Decay Time

The time required for the peak current to decay from 90% to 10% (using the

steady-state current as baseline) in forced desensitization from a 55s application of 300

μM ACh was calculated in Clampfit. The 90-10% decay time in cells expressing the 1:3

α3β2 ratio (n=2) averaged 20074.33 ms ± 5026.72. The cells expressing α3β2 in a 1:1

ratio (n=4) produced an average forced desensitization 90-10% decay time of 16647.24

ms ± 674.87. The 3:1 α3β2 expression group (n=6) produced an average forced

desensitization 90-10% decay time of 13014.86 ms ± 717.14. This was significantly

different from the average decay time in cells expressing the 1:3 ratio of α3β2 subunits,

according to a two-tailed t-test (P=0.040) (Tables 5a & b, Figure 16).

Decay Constants in Forced Desensitization

The decay constant (tau) was calculated in Clampfit for each component of the

forced desensitization curves elicited from a 55s application of 300 μM ACh. The largest

tau for each of the forced desensitization curves was averaged for each expression group

for statistical analysis. The average decay taus for the 1:3, 1:1, and 3:1 α3β2 expression

groups were 10687.23 ms ± 76.63, 11823.91 ms ± 2525.49, and 11368.12 ms ± 3317.60,

respectively (Table 6a). A two-tailed t-test revealed that there was no significant

difference between the average taus for the 1:3 and 3:1 expression groups (P=0.914)

(Table 6b, Figure 17).

Dose-Response Curves

It has been previously demonstrated that differential stoichiometric expression of heteromeric αβ nAChRs can greatly affect receptor sensitivity to agonist (Zwart and Vijverberg 1998; Nelson, Kuryatov et al. 2003; Lopez-Hernandez, Sanchez-Padilla et al. 2004; Moroni, Zwart et al. 2006). Full dose-response curves were compiled at ACh concentrations of 1 μM, 10 μM, 100 μM, 300 μM, 1 mM, and 10 mM (Figure 11a). Current responses were also elicited from 1s applications of 30 mM ACh to verify that the maximally effective concentration was 10 mM ACh for each different expression group (1:3, 1:1, and 3:1). The average % of the peak current elicited from a 1s application of 30 mM ACh was 96.09% for the 1:3 expression group (n=9), 75.77% for the 1:1 expression group (n=9), and 97.97% for the 3:1 expression group (n=12) (Figure 11b). The 30 mM data were not included in the dose-response curves for the sake of maximally fitting the curve to the data points.

Confident that a 1s application of 10mM ACh produced the maximal response, all other responses to the different ACh concentrations could be normalized to the peak current from the application of 10 mM ACh on the same cell. The average of 3 replicates at each ACh concentration in the dose-response curve was taken to compile a list of 45 averages for the 1:3 dose-response curve, 40 averages for the 1:1 dose-response curve, and 45 averages for the 3:1 dose-response curve. The average % of peak current at each ACh concentration was then taken from the averages of the replicates to provide 6 points for the dose-response curves in each of the expression groups. Dose-response analysis and graphing was performed on Prism ver. 4.03 (GraphPad Software, San Diego CA).

The EC_{50} of each dose-response curve was calculated in Prism. Cells injected with $\alpha3\beta2$ mRNA in a 1:3 ratio showed the highest sensitivity to ACh with an EC_{50} of 129.5 μM ACh. The EC_{50} of the 1:1 $\alpha3\beta2$ expression group increased 60.2 μM to 189.7 μM ACh. The 3:1 expression group showed the lowest sensitivity to ACh with an EC_{50} of 245.5 μM. While a t-test showed no significant difference between the EC_{50} values of the 1:3 and 3:1 expression groups (P=0.4656), it is interesting to note that the pattern of receptor sensitivity decreases in almost even increments from 1:3 to 1:1 to 3:1. For a summary of all results, see the consolidated results table (Table 7).

TABLES AND FIGURES
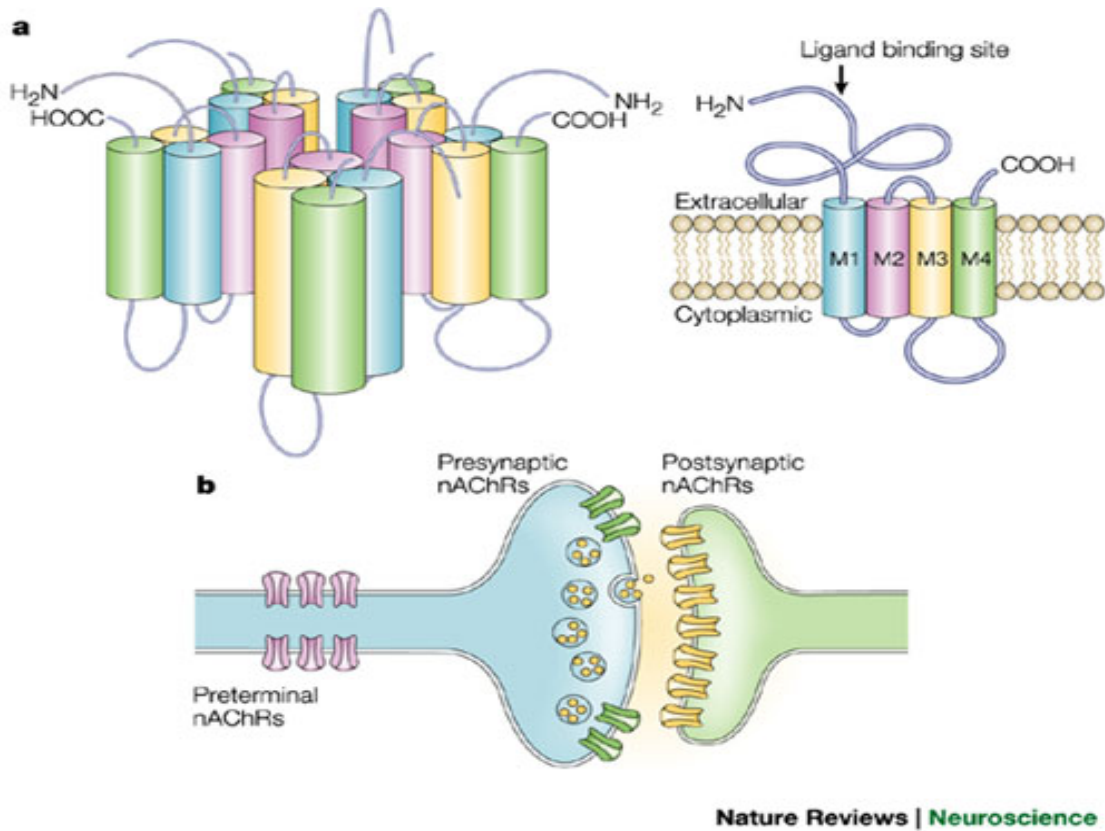
Figure 1a. Pentameric assembly of nAChR subunits (Left). General structure of an individual nAChR subunit.
b. Pre-, post-, and non-synaptic location of nAChRs (illustration from Laviolette and van der Kooy 2004).
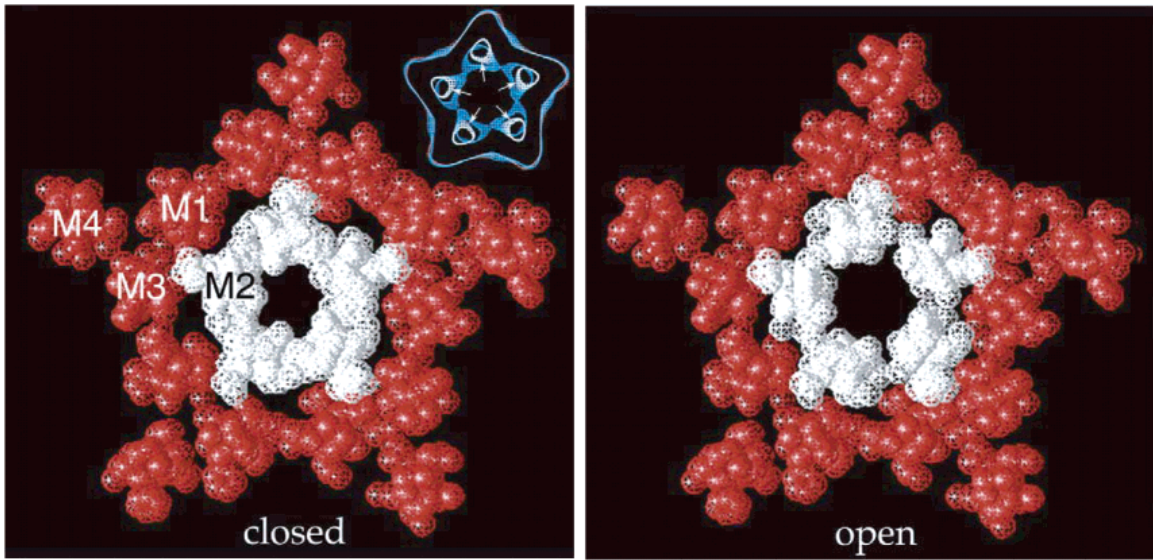
Figure 2. Ion pore of the Torpedo nAChR. Transmembrane regions for one of the five subunits marked M1-M4. Opening of the ion channel: cross-sections of the closed and open ion channels in the middle of the membrane.(Jensen, Frolund et al. 2005)
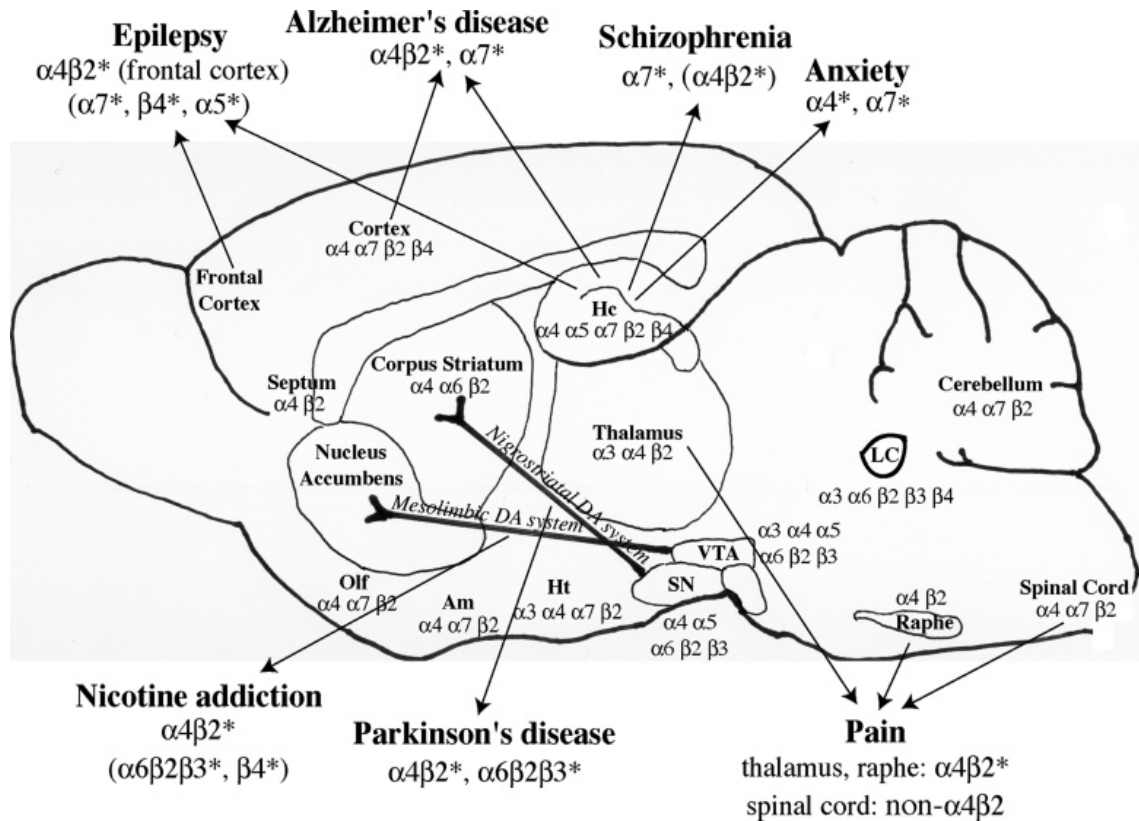
Figure 3. Distribution of nAChR subunits in the rodent brain. The nAChR subunits predominantly expressed in selected CNS regions are shown, and the nAChRs proposed as potential therapeutic targets in various disorders are indicated: Hc, hippocampus; Ht, hypothalamus; VTA, ventral tegmental area; SN, substantia nigra; Olf, olfactory region; Am, amygdala; LC, locus coeruleus. (Jensen, Frolund et al. 2005)

Rat Hippocampus
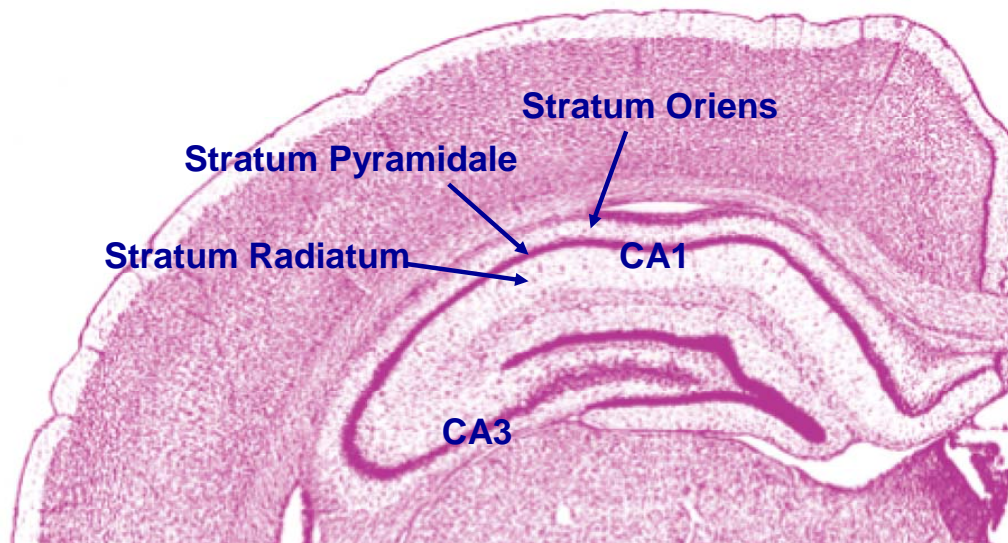
Figure 4. Rat hippocampal slice showing the rough anatomy of the hippocampus. Arrows indicate areas where interneurons were aspirated for PCR analysis (Photo from (Swanson 1998).
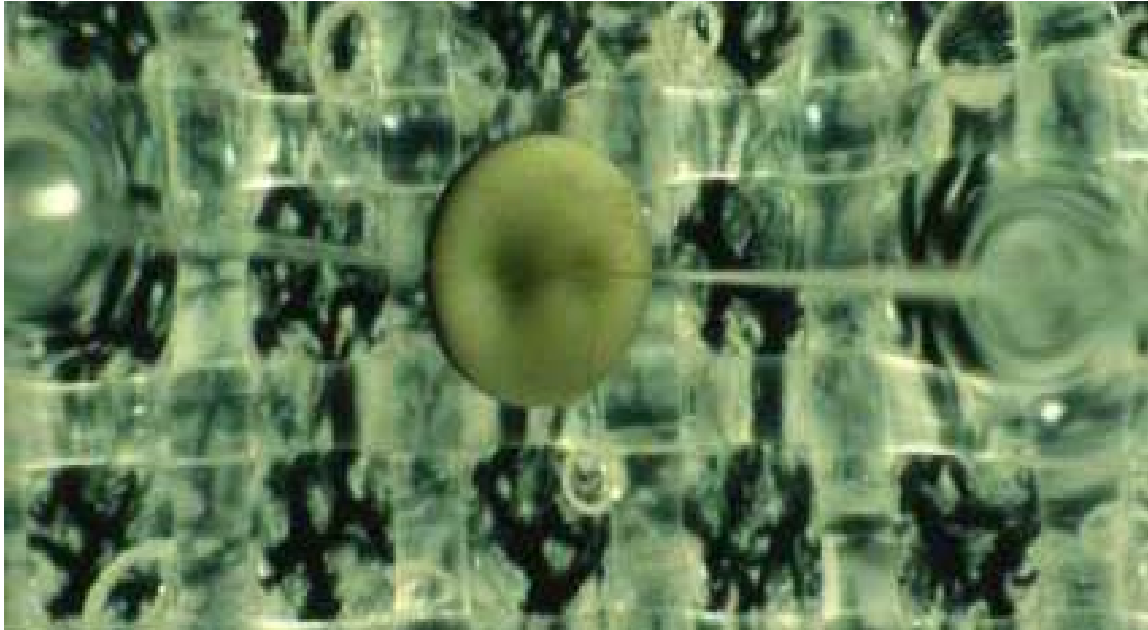
Figure 5. Example of a two-electrode voltage clamp setup for current recordings on *Xenopus* oocytes (Photo by: Mizukawa 2008).

Neuronal nAChR Subunit Co-Expression in Individual Interneurons

43%	of Cells Co-expressed α3 and β2
38%	of Cells Co-expressed α7 and β2
33%	of Cells Co-expressed α3 and β4
27%	of Cells Co-expressed α4 and β2
24%	of Cells Co-expressed α2 and β2
22%	of Cells Co-expressed α7 and β4
20%	of Cells Co-expressed α2 and β4
15%	of Cells Co-expressed α4 and β4

Figure 6. The most common mRNA combinations of two neuronal nAChR subunits observed in individual hippocampal CA1 interneurons using single-cell quantitative RT-PCR (n=79).
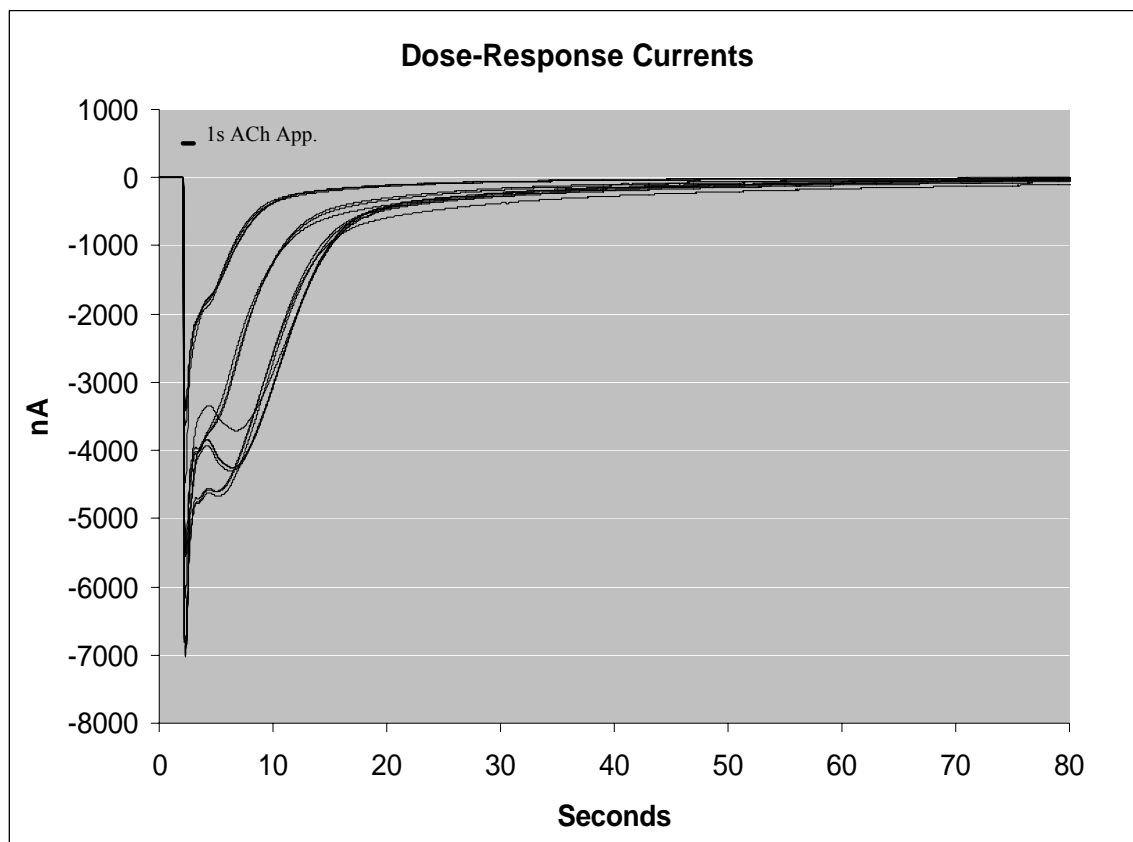
Figure 7. Example of currents in the dose-response protocol. Currents seen above were elicited from 3 consecutive 1s applications of 100 μM, 1 mM, 10 mM, and 30 mM ACh waiting 2 minutes between ACh applications.

26
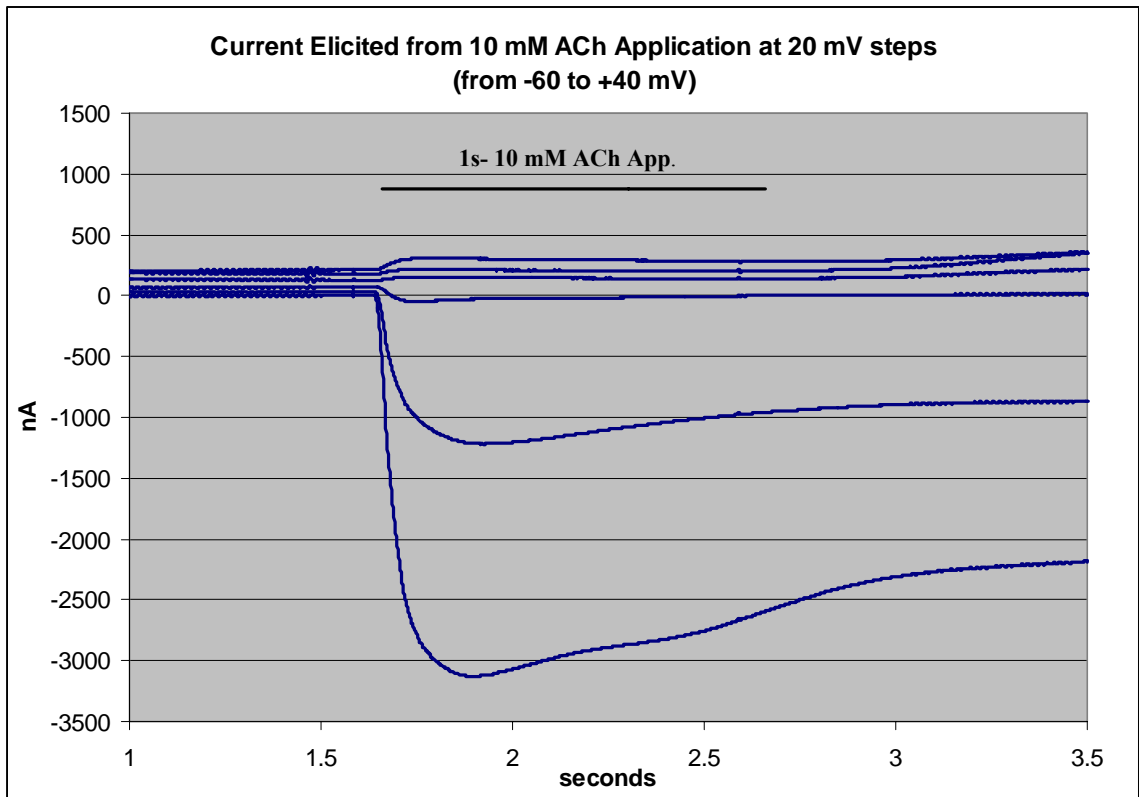
Figure 8. Example of currents in the IV protocol. Currents seen above were in response to a 1s application of 10 mM ACh at holding potentials of -60, -40, -20, 0, 20, 40 mV waiting 2 minutes between ACh applications.

IV Plot

$R^2 = 0.9997$
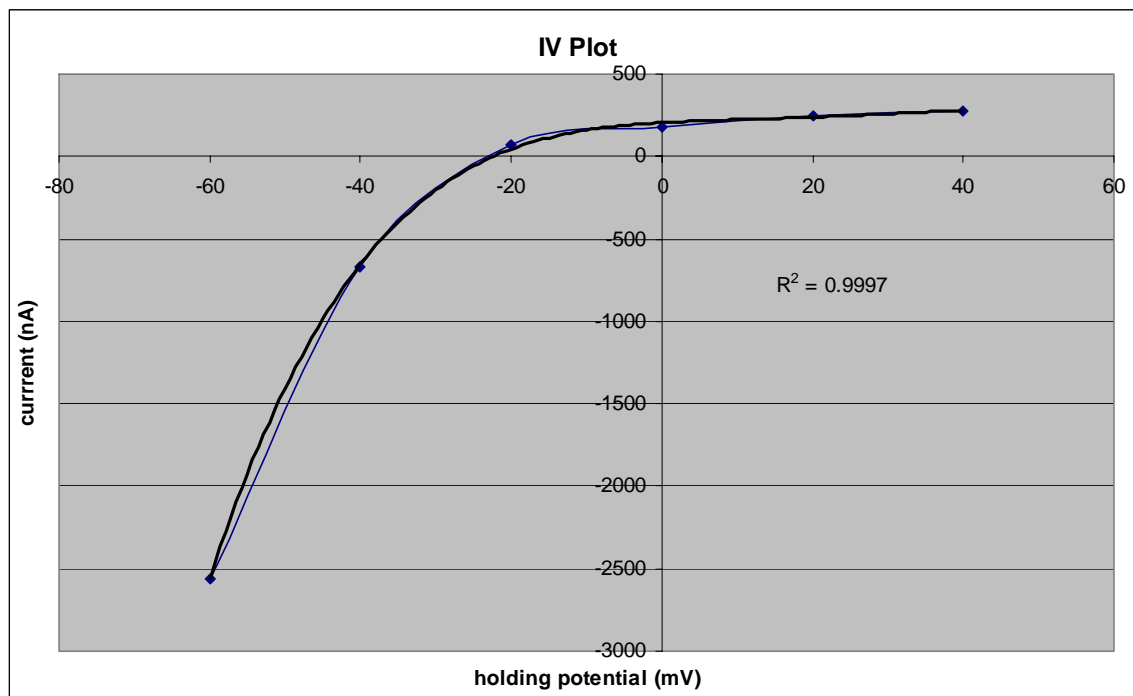
3:1

Figure 9. IV plot showing rectification of a 3:1 α3β2 nAChR in *Xenopus* oocytes with holding potentials of -60, -40, -20, 0, 20, 40 mV. Each current was elicited from a 1s application of 10 mM ACh.

28

Forced Desensitization Following Extended ACh Application

55s- 300 µM ACh App
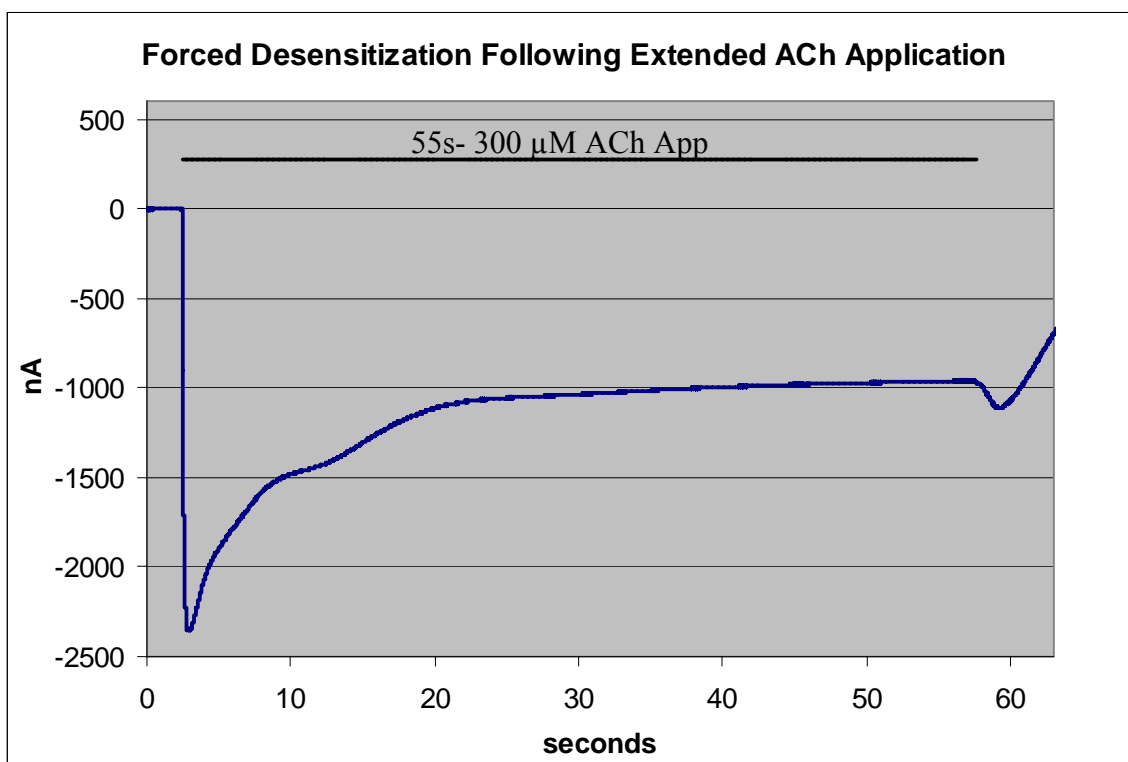
Figure 10. Example of current in forced desensitization. 300 µM ACh was applied constantly over a 55s period to force the receptor into a desensitized state.

11a.
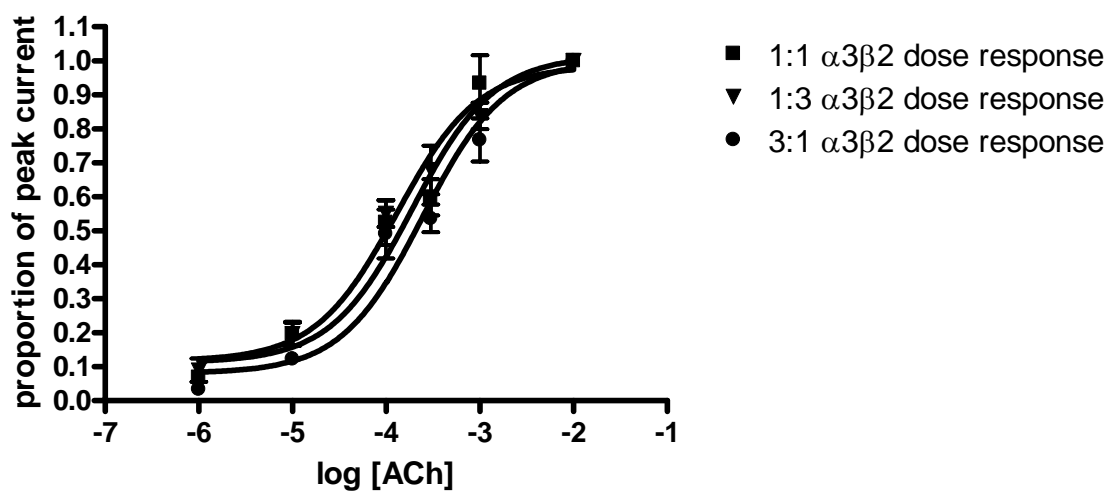
b.

	1:3	1:1	3:1
EC50	0.0001295	0.0001897	0.0002455
R²	0.9154	0.9218	0.9206
Total number of values	45	40	45

Figure 11a. Dose-response curves for (from left to right) 1:3, 1:1, and 3:1 α3β2 nAChRs. Six concentrations (1 μM, 10 μM, 100 μM, 300 μM, 1 mM, 10 mM) of ACh were normalized to the peak currents elicited from a 1s application of 10 mM ACh. Points for the dose-response curves were taken from the averages of the % of peak at each given dose for each respective stoichiometric expression ratio.
b. EC$_{50}$ values for each of the three dose-response curves. R^2 values for the curve fit of the dose-responses are also listed with the number of values used to calculate each curve.

10-90% Rise Times			
	1:3	*3:1*	*1:1*
Mean (msec)	222	98	144
Standard Error	48	10	30
Median	144	87	91
Standard Deviation	302	62	189
Sample Variance	91364	3900	35726
Range	1312	324	1022
Minimum	39	32	36
Maximum	1351	357	1058
Count	40	43	39

Table 1a. Column statistics for the rise times from 10% to 90% of the peak current elicited from a 1s application of 10 mM ACh.

t-Test: Two-Sample Assuming Equal Variances		
	1:3	*3:1*
Mean (msec)	222	98
Variance	91364	3900
Observations	40	43
Pooled Variance	46013	
Hypothesized Mean Difference	0	
Df	81	
t Stat	3	
P(T<=t) one-tail	0.005	
t Critical one-tail	1.66	
P(T<=t) two-tail	0.010	significant
t Critical two-tail	1.99	

Table 1b. Two-tailed t-test for difference in the means of the 10-90% rise times of the 1:3 and 3:1 α3 β2 groups. (significance = P<0.05).
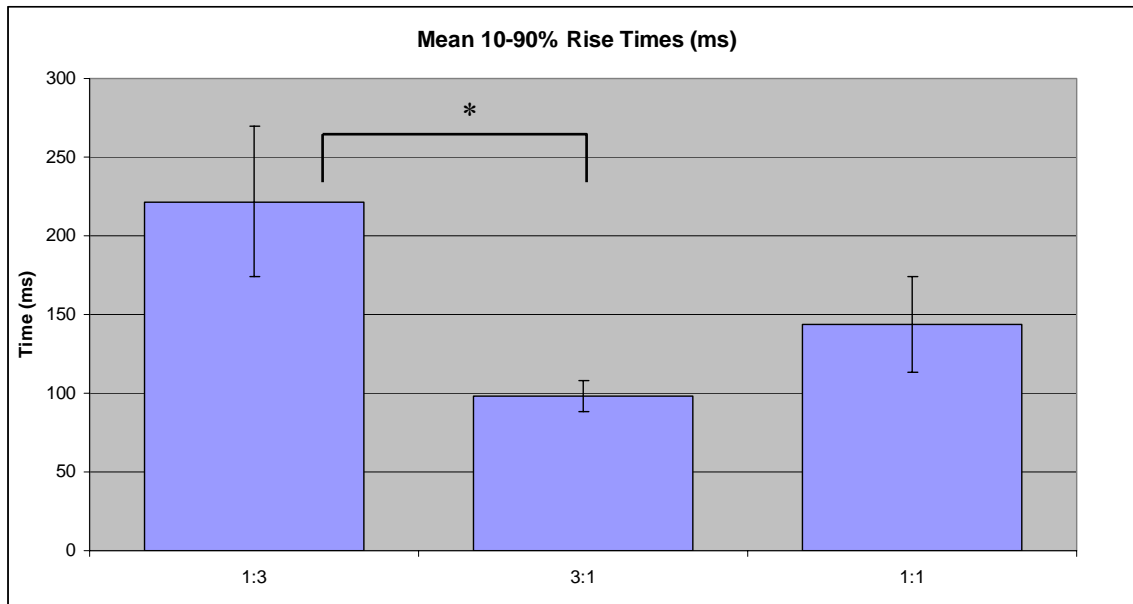
Figure 12. Average of the 10%-90% rise times elicited from a 1s application of 10 mM ACh (* indicates P<.01 significance, two-tailed t-test).

Reversal Potentials			
	1:3	*1:1*	*3:1*
Mean (mV)	-25	-18	-17
Standard Error	4	1	2
Median	-24	-17	-17
Standard Deviation	6	3	4
Sample Variance	40	7	20
Range	12	6	12
Minimum	-32	-21	-22
Maximum	-19	-16	-11
Sum	-74	-70	-85
Count	3	4	5

Table 2a. Column statistics for the reversal potentials from current elicited from a 1s application of 10 mM ACh at mV steps of -60, -40, -20, 0, 20, 40 mV.

t-Test: Two-Sample Assuming Equal Variances		
	1:3	*3:1*
Mean (mV)	-25	-17
Variance	40	20
Observations	3	5
Pooled Variance	26	
Hypothesized Mean Difference	0	
Df	6	
t Stat	2	
P(T<=t) one-tail	0.04	
t Critical one-tail	1.9	
P(T<=t) two-tail	0.09	not sig.
t Critical two-tail	2.4	

Table 2b. Two-tailed t-test for difference in the means of the reversal potentials of the 1:3 and 3:1 α3 β2 groups. (significance = P<0.05).
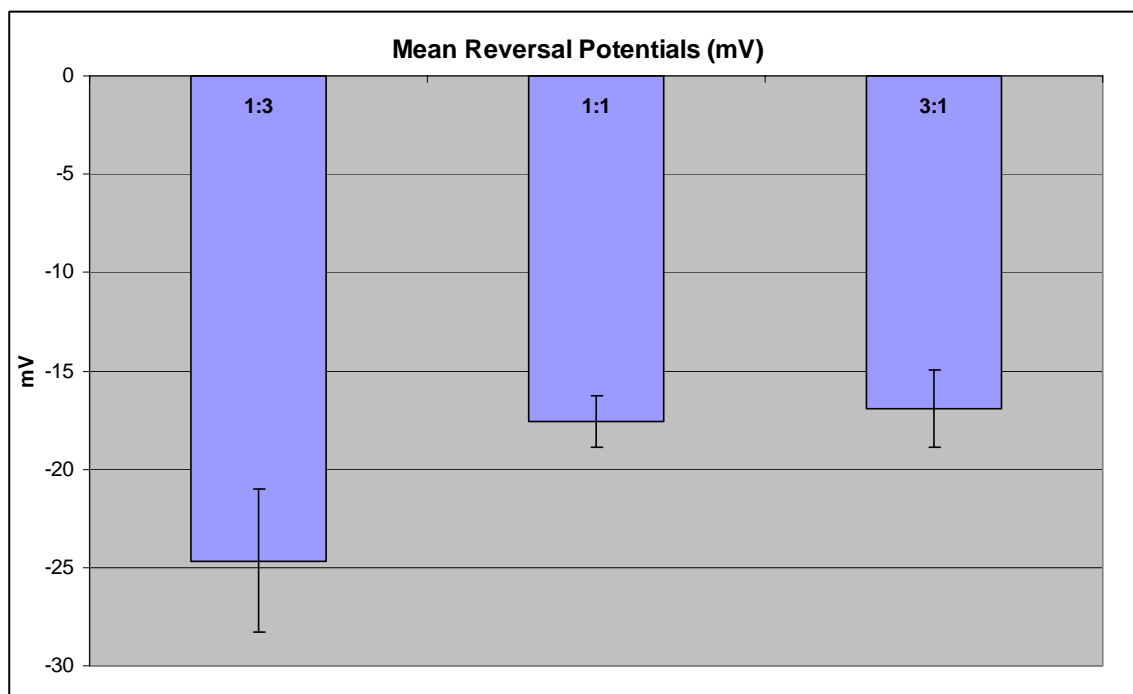
Figure 13. Average reversal potentials for all groups; 1:3, 1:1, 3:1 (significance = P<0.05).

Steady State Current Compared to Peak Current with Extended Agonist Application (Forced Desensitization)			
	1:3	*1:1*	*3:1*
Mean (proportion of peak)	0.394	0.414	0.253
Standard Error	0.020	0.096	0.028
Median	0.394	0.368	0.234
Standard Deviation	0.029	0.192	0.068
Sample Variance	0.001	0.037	0.005
Range	0.041	0.441	0.161
Minimum	0.373	0.240	0.177
Maximum	0.414	0.681	0.338
Sum	0.787	1.656	1.517
Count	2	4	6

Table 3a. Column statistics for the steady state current compared to the peak current from a 55s application of 10 mM ACh.

t-Test: Two-Sample Assuming Equal Variances		
	1:3	*3:1*
Mean (proportion of peak)	0.394	0.253
Variance	0.0008	0.0047
Observations	2	6
Pooled Variance	0.004	
Hypothesized Mean Difference	0	
df	6	
t Stat	2.719	
P(T<=t) one-tail	0.017	
t Critical one-tail	1.943	
P(T<=t) two-tail	0.035	significant
t Critical two-tail	2.447	

Table 3b. Two-tailed t-test for difference in the means of the steady state current compared to the peak current from a 55s application of 10 mM ACh.

% of Peak After Decay in Forced Desensitization
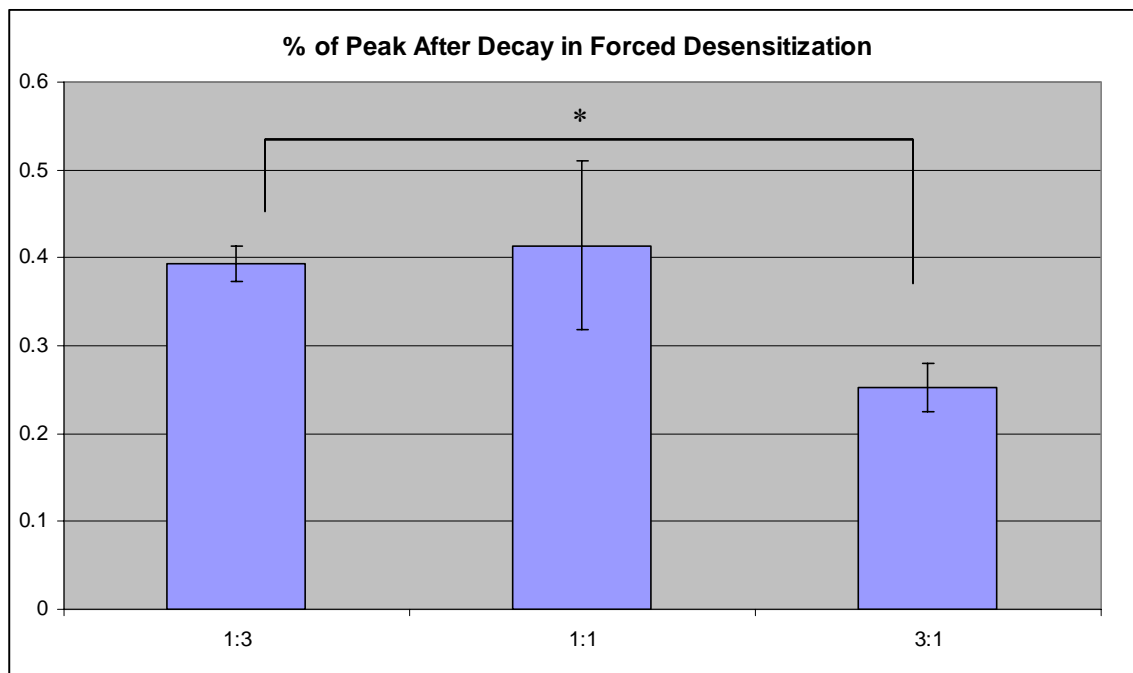
Figure 14. Average steady state current compared to peak current in forced desensitization (* indicates significance, P < 0.05).

# of Exponents Used for Curve Fit			
	1:3	*1:1*	*3:1*
Mean	1.3	2.5	3.3
Standard Error	0.3	0.9	0.8
Median	1	2	3
Mode	1	2	2
Standard Deviation	0.6	1.7	2.0
Sample Variance	0.3	3	3.9
Range	1	4	5
Minimum	1	1	1
Maximum	2	5	6
Sum	4	10	20
Count	2	4	6

Table 4a. Column statistics for the # of exponents used to curve fit the forced desensitization decay.

t-Test: Two-Sample Assuming Equal Variances		
	1:3	*3:1*
Mean	1.3	3.3
Variance	0.3	3.9
Observations	3	6
Pooled Variance	2.9	
Hypothesized Mean Difference	0	
Df	7	
t Stat	-1.7	
P(T<=t) one-tail	0.07	
t Critical one-tail	1.9	
P(T<=t) two-tail	0.14	not sig.
t Critical two-tail	2.4	

Table 4b. Two-tailed t-test for difference in the means of the # of exponents used to curve fit the forced desensitization decay.
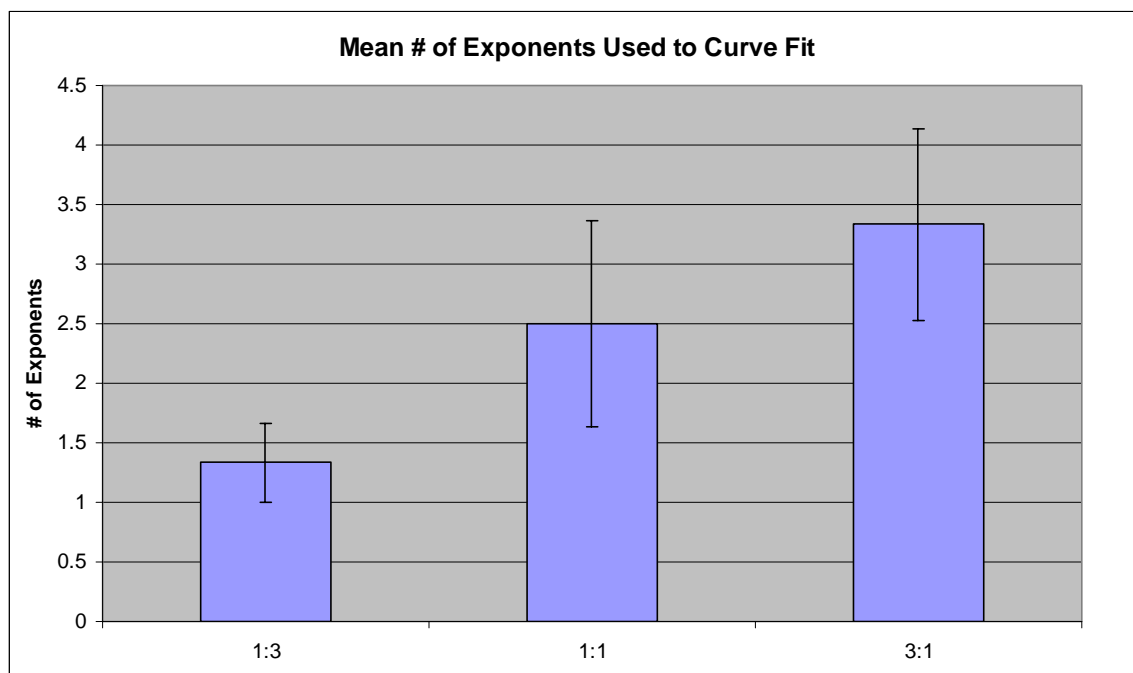
Figure 15. Average # of exponents used to fit the decay of the forced desensitization (significance = P< 0.05).

90-10% Decay Time			
	1:3	*1:1*	*3:1*
Mean (msec)	20074	16647	13015
Standard Error	5027	675	717
Median	20074	17115	12696
Standard Deviation	7109	1350	1757
Sample Variance	50536000	1821800	3086000
Range	10053	2956	5176
Minimum	15048	14701	11170
Maximum	25101	17657	16347
Sum	40149	66589	78089
Count	2	4	6

Table 5a. Column statistics for the decay times from 90% of the peak current to 10% of the steady state current during forced desensitization from 55s of 10 mM ACh.

t-Test: Two-Sample Assuming Equal Variances		
	1:3	*3:1*
Mean (msec)	20074	13015
Variance	50536000	3086000
Observations	2	6
Pooled Variance	10994000	
Hypothesized Mean Difference	0	
Df	6	
t Stat	2.6	
P(T<=t) one-tail	0.02	
t Critical one-tail	1.9	
P(T<=t) two-tail	0.04	significant
t Critical two-tail	2.4	

Table 5b. Two-tailed t-test for difference in the means of decay times from 90% of the peak current to 10% of the steady state current during forced desensitization from 55s of 10 mM ACh (significance = P<0.05).
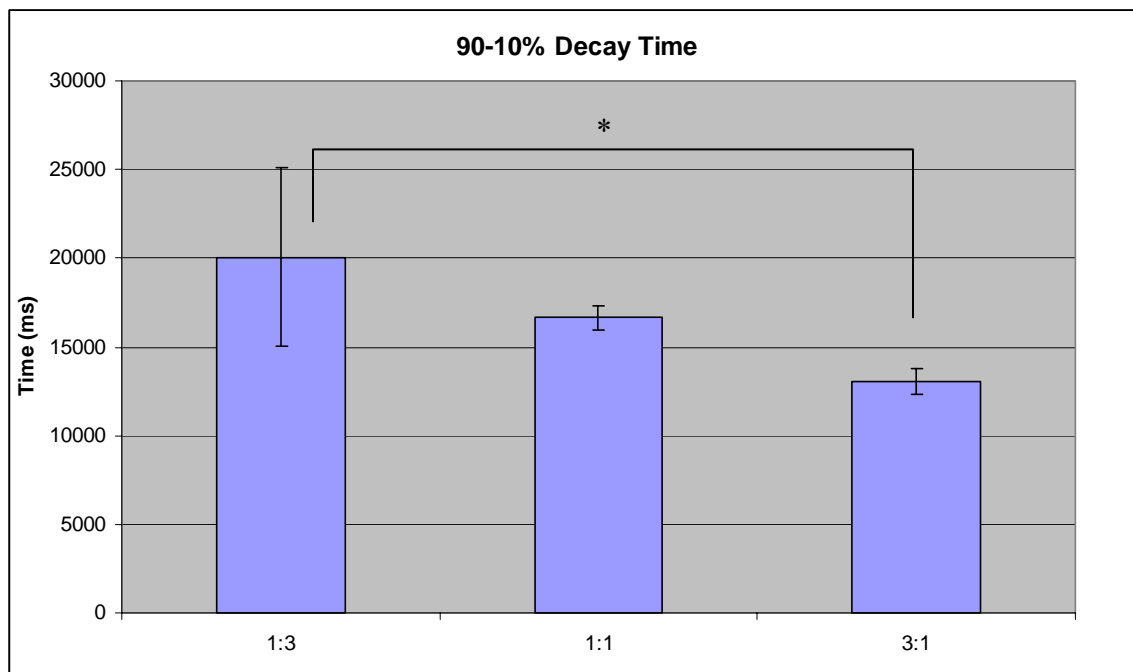
Figure 16. **Average decay times from 90% of the peak current to 10% of the steady state current during forced desensitization from 55s of 10 mM ACh (* indicates significance, P<0.05).**

Decay Tau1			
	1:3	*1:1*	*3:1*
Mean (msec)	10687	11824	11368
Standard Error	77	2525	3318
Median	10687	12106	9188
Standard Deviation	108	5050	8126
Sample Variance	11744	25512438	66038900
Range	153	9842	21807
Minimum	10610	6620	5750
Maximum	10760	16460	27550
Sum	21370	47300	68210
Count	2	4	6

Table 6a. Column statistics for the decay tau from the forced desensitization decay curves.

t-Test: Two-Sample Assuming Equal Variances		
	1:3	*3:1*
Mean (msec)	10687	11368
Variance	11744	66038900
Observations	2	6
Pooled Variance	55034374	
Hypothesized Mean Difference	0	
Df	6	
t Stat	-0.1	
P(T<=t) one-tail	0.5	
t Critical one-tail	2	
P(T<=t) two-tail	0.9	not sig.
t Critical two-tail	2	

Table 6b. Two-tailed t-test for difference in the mean decay tau values from the forced desensitization decay curves.
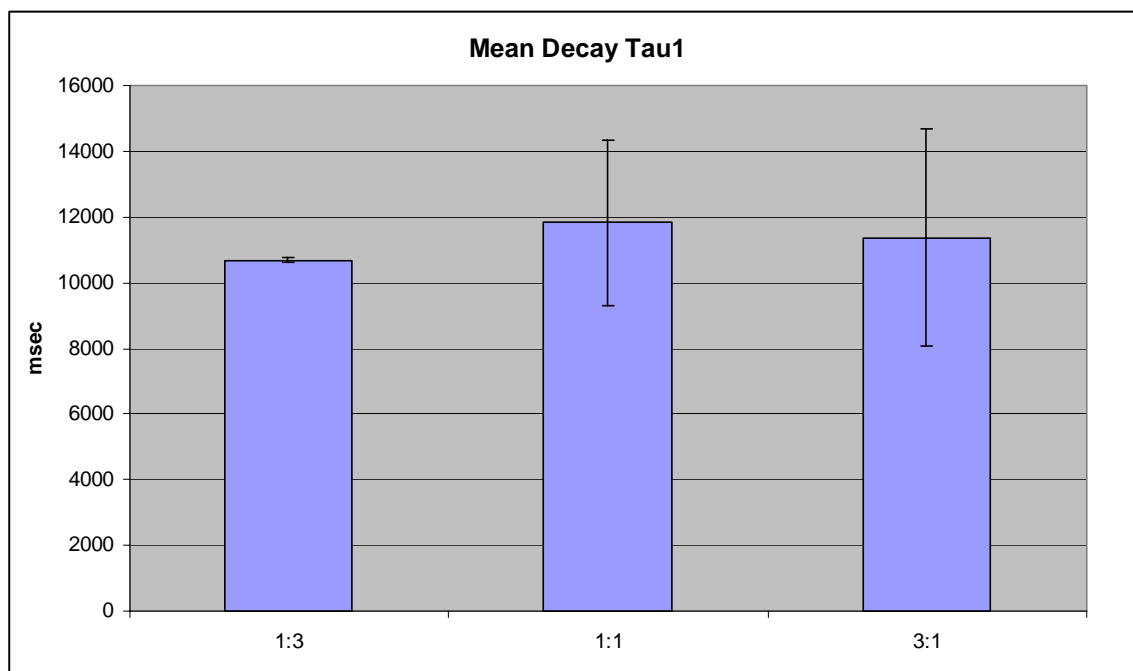
Figure 17. Average of the decay tau values from the forced desensitization decay curves (significance = P<0.05).

	1:3	3:1	1:1	Significance (1:3, 3:1)
10-90% Rise Time (msec)	222	98	144	P=0.010, significant
Reversal Potential (mV)	-25	-17	-18	P=0.09, not sig.
Steady State Current (%)	0.394	0.253	0.414	P=0.035, significant
# of Exponents in Decay Fit	1.3	3.3	2.5	P=0.14, not sig.
90-10% Decay Time (msec)	20074	13015	16647	P=0.04, significant
Decay Tau (msec)	10687	11368	11824	P=0.9, not sig.
EC50 [M]	0.00013	0.00025	0.00019	P=0.47, not sig.

Table 7. Consolidated table of results. Values reported as averages. P values for two-tailed t-tests between the 1:3 and 3:1 expression groups provided.

DISCUSSION

Neuronal nAChRs are expressed throughout the PNS and CNS, and are involved in a wide variety of physiological processes (Ortells 1995; Albuquerque, Pereira et al. 1996; Changeux, Bessis et al. 1996; Newhouse, Potter et al. 1997; Dani JA 2007). The α3 subunit is widely expressed in the PNS, forming heteromeric receptors commonly with the β4 subunit (Paterson and Nordberg 2000; Jensen, Frolund et al. 2005). However, the α3 subunit has not been found to be widely expressed in the CNS.   The prevailing theory suggests that approximately 90% of neuronal nAChRs in the CNS are α4β2 receptors, while the vast majority of the remaining nAChRs expressed in the CNS are α7 homomers (Jensen, Frolund et al. 2005). Therefore, the α3β4 and the α4β2 receptors have been characterized quite well, due to the overwhelming evidence of expression in the PNS and CNS respectively. However, the α3β2 receptor has not shown much expression in the body overall, so it is relatively uncharacterized by comparison.

From the PCR data, it was surprising to find that; 1) the rat CA1 hippocampal interneurons expressed α3 at such high levels, and 2) the α3β2 co-expression rate in the hippocampus surpassed that of any other two-way subunit combination, including α4β2. According to Welch 2008, the β2 subunit was expressed in 100% of the 106 whole hippocampus tissue samples taken from Wistar rats ranging from 10 to 90 days in age, while the α3 and α4 subunits were both expressed in over 90% of the same samples. The range of expression of these subunits in the hippocampus is similarly high. However, the relative expression levels of each subunit are quite different. The α4 subunit, though widely expressed in the hippocampus, showed a relatively low level of expression compared to all other subunits save the β3 subunit. The α3 subunit demonstrated a

relative fold expression generally three times higher than the α4 subunit in the hippocampus over the development of Wistar rats into adolescence. The β2 subunit enjoyed the second highest level of expression of all subunits, just below the α5 subunit (Welch 2008). Therefore, the α3 and β2 subunits were shown to be both widely and highly expressed in the rat hippocampus throughout development. While the PCR data presented in this thesis are taken specifically from individual CA1 hippocampal interneurons and not the whole hippocampus, the data from the whole hippocampus (Welch 2008) seem to support our findings extremely well. Because α4β2 containing receptors have been shown to be widely expressed throughout the brain, there has been an assumption that this subtype is one of the most prevalent in the hippocampus as well. Our findings indicate that this assumption may be incorrect, with α3β2 containing receptors demonstrating to be more predominant in the hippocampus (Wada, Wada et al. 1989; Alkondon and Albuquerque 1993; Jones and Yakel 1997; McQuiston and Madison 1999; Jensen, Frolund et al. 2005).

The co-expression rate of the α3 and β2 subunits in hippocampal interneurons was not only the highest of all two-way subunit combinations in the hippocampal interneurons, but it also proved to be 7.6% higher than expected (observed co-expression 43%, expected 35.4%), based on the individual expression rates of α3 and β2 (59.5% for both α3 and β2 (i.e., 0.595 X 0.595 = 0.354 or 35.4% for the expected co-expression rate). Moreover, 72% of interneurons that expressed α3 also expressed β2 and vice versa. These data suggest a definite tendency for the α3 and β2 subunits to be co-expressed in individual neurons. Due to the apparent prevalence of α3β2 receptors in hippocampal interneurons and their lack of prevalence elsewhere in the body, the α3β2 receptors are an

ideal target of interest for research involving hippocampal pathologies where neuronal

nAChRs are implicated as being involved (i.e.- Alzheimer's disease AD, schizophrenia,

etc.) (Court 2001; Woodruff-Pak DS 2002; Bourin, Ripoll et al. 2003).

Not only did our PCR data show the high rate of α3β2 co-expression in

hippocampal interneurons, but the relative stoichiometric expression ratios of α3:β2 were

measured as well. Of the 34 interneurons that co-expressed the α3 and β2 subunits, 15 of

them expressed α3 more than β2 by an average of 2.5 fold. The remaining 19 cells that

co-expressed the α3 and β2 subunits expressed the β2 subunit more than α3 by an average

of 3.3 fold. These data suggest that the 1:3 and 3:1 α3β2 expression groups might be

more physiologically relevant to future hippocampal studies. It also shows a slight

favoring of the receptors expressing more β2 than α3.

It is necessary to note that a plasmid containing the human α3 gene was combined

with a plasmid containing the rat β2 gene for expression in the oocytes used for voltage

clamp recordings. It is evident that the human α3 subunit readily associates with the rat

β2 subunit to form fully functional heteropentamers in terms of cationic selectivity,

current rectification, current conductance, agonist binding, and desensitization. Because

of the high homology between subunits (NCBI BLASTN pairwise alignment = 88%

identity for nucleotide sequences, BLASTP pairwise alignment = 95% identity for the

two protein sequences), we expected that the disparity in species would not inhibit the

formation of functional receptors. However, it would be interesting to see if rat α3β2

and/or human α3β2 receptors would produce the same kinetics, agonist affinity, and

agonist sensitivity as the chimeric combination we produced in our experiments.

All three expression groups (1:3, 1:1, and 3:1 α3β2) produced functional acetylcholine receptors on the oocyte membrane. The cells that were injected with 1:3 α3β2 subunit mRNA expressed receptors with significantly different kinetics than the receptors expressed by the cells injected with α3β2 mRNA in the 3:1 ratio. The receptors formed by the 1:3 α3β2 expression group demonstrated significantly higher values for average 10-90% rise time, average 90-10% decay time during forced desensitization, and average steady state current compared to peak current in forced desensitization than the 3:1 α3β2 expression group (Table 7). The forced desensitization decay data is particularly interesting as it indicates a slower and lesser degree of desensitization in the 1:3 α3β2 expression group than the 3:1 group. The significantly different kinetics in the receptors expressed by the 1:3 group and the 3:1 group indicate that the α3 and β2 subunits in these stoichiometric ratios produce different receptor populations.

The different receptors did not vary significantly in their reversal potentials. This was expected because the pipette solution, bath solution, and temperature were kept relatively constant throughout all of the experiments. All three expression groups did display considerable inward negative current rectification (Figure 9). The receptors expressed by the 1:3 α3β2 group also did not significantly differ from the receptors from the 3:1 group with respect to decay tau and # exponents used to curve fit the decay in forced desensitization. The similarity in decay tau suggests that the main component of the decay during forced desensitization in the two receptor types is brought about by a similar mechanism.

The # of exponents used to curve fit the decay in forced desensitization was not significantly different between the distinct expression groups. The number of exponents

used for the decay curve fit ranged from 1 to 6 exponents, while the average was 2.7. As the # of exponents used to fit the decay curve increases, so does the complexity of the curve. The multiple exponents used to fit the forced desensitization decay curves in our experiments can employ one of two explanations. Different populations of receptors can demonstrate different decay rates, or different populations of receptors can be expressed within the same expression group. For example, while the 1:3 expression group would favor expression of a higher number of β subunits than α subunits, they could form pentamers with 1-α subunit and 4-β subunits or 2-α subunits and 3-β subunits. Different populations of receptors within the same expression group may also be explained through different specific subunit conformations. For example, though two receptors may both contain two α3 subunits and three β2 subunits, one receptor may assemble to form a functional channel with a specific conformation of α3α3β2β2β2, while a different receptor may assemble in a specific conformation of α3β2α3β2β2.

The multiple exponents in the forced desensitization decay curve may also be explained through multiple receptor states. In general, nAChRs are found in an active, inactive, or desensitized state. However, contemporary models have proposed another "resting" state or multiple desensitized states (Miyazawa, Fujiyoshi et al. 2003; Giniatullin, Nistri et al. 2005; Gay and Yakel 2007). The receptors may be shifting between desensitization states throughout the 55s ACh application to cause the complex decay curve.

We established that the different expression groups produced distinct populations of nAChRs based on their significantly different channel kinetics. Many previous experiments have shown a shift in EC_{50} and agonist sensitivity with differential

48

stoichiometric subunit expression (Zwart and Vijverberg 1998; Nelson, Kuryatov et al. 2003; Lopez-Hernandez, Sanchez-Padilla et al. 2004). In our experiments, there was no significant difference between EC_{50} values of the different expression groups. However, we noticed a definite pattern of change in EC_{50} values for the different groups as the expression ratio of α3 and β2 changed. More than 120 currents at six different ACh concentrations were normalized to peak currents and averaged to form the dose-response curve of each expression group. The EC_{50} values were almost evenly-spaced between expression groups, differing 60 μM between the 1:3 and 1:1 expression groups, and 56 μM between the 1:1 and 3:1 expression groups. The trend observed in our experiments showed a greater sensitivity to ACh as the expression of the α3 subunit increased in comparison to the expression of the β2 subunit. This observation seems to contradict the pattern observed in other studies where an increase of β2 expression in relation to α4 increases the receptor's sensitivity to ACh. This disparity may be due to specific differences in the different subunits.

Future studies for further characterization of α3and β2 subunit containing receptors could take many directions. Many different pharmacological studies can be performed. For example, Luetje and Patrick used α3β2 and α2β2 receptors to show the different relative sensitivities to application of ACh and nicotine (Luetje and Patrick 1991). They found that while application of ACh elicited larger currents in α3β2 receptors than α2β2 receptors, the opposite was true about nicotine. Equal application of nicotine actually induced larger currents in α2β2 receptors than α3β2 receptors. This could be further investigated to see if chronic exposure to nicotine increases or decreases the expression of α3β2 receptors. Nelson et al. found that long-term exposure to nicotine

up-regulates the expression of α4β2 receptors with the stoichiometric expression ratio of 2 α subunits to 3 β subunits and decreased all other stoichiometric expression (Nelson, Kuryatov et al. 2003). Interestingly, they found that the 2:3 α4β2 receptor had the highest sensitivity to ACh out of all the other stoichiometric formations.

Other nAChR agonists and antagonists may be used as well to compile a full dose-response/EC_{50}/IC_{50} profile for the different pharmacological agents (i.e.- nicotine, cytisine, choline, epibatidine, 1,1-dimethyl-4-phenylpiperazinium, etc.) A useful application of an antagonist study could possibly be found in α-conotoxin MII. This toxin, isolated from the cocktail of toxins in cone snails, has been shown to specifically block α3β2 and α6β2 receptors. Our PCR data showed absolutely no expression of the α6 subunit in any of the CA1 hippocampal interneurons we analyzed. If α3β2 receptors truly are prevalent and functional in rat hippocampal interneurons, a blockade of agonist induced current would be observed with addition of α-conotoxin MII in an *in vivo* voltage-clamp recording.

REFERENCES

Albuquerque, E. X., E. F. Pereira, et al. (1996). "Nicotinic acetylcholine receptors on hippocampal neurons: cell compartment-specific expression and modulatory control of channel activity." Prog Brain Res **109**: 111-24.

Alkondon, M. and E. X. Albuquerque (1993). "Diversity of nicotinic acetylcholine receptors in rat hippocampal neurons. I. Pharmacological and functional evidence for distinct structural subtypes." J Pharmacol Exp Ther **265**(3): 1455-73.

Anand R, C. W., Schoepfer R, Whiting P, Lindstrom J. (1991). "Neuronal Nicotinic Acetylcholine Receptors Expressed in Xenopus

Oocytes Have a Pentameric Quaternary Structur." J Biol Chem **266**(17): 11192-8.

Boorman, J. P., P. J. Groot-Kormelink, et al. (2000). "Stoichiometry of human recombinant neuronal nicotinic receptors containing the b3 subunit expressed in Xenopus oocytes." J Physiol **529 Pt 3**: 565-77.

Bourin, M., N. Ripoll, et al. (2003). "Nicotinic receptors and Alzheimer's disease." Curr Med Res Opin **19**(3): 169-77.

Burgon, R. M. (2006). Classification of Neuronal Nicotinic Acetylcholine Receptors in Rat CA1 Hippocampal Interneuron Subpopulations Defined by Calcium-Binding Protein. Physiology and Developmental Biology. Provo, Brigham Young University. **Master of Science:** 38.

Changeux, J.-P. and S. J. Edelstein (2005). Nicotinic acetylcholine receptors : from molecular biology to cognition. New York, Odile Jacob.

Changeux, J. P., D. Bertrand, et al. (1998). "Brain nicotinic receptors: structure and regulation, role in learning and reinforcement." Brain Res Brain Res Rev **26**(2-3): 198-216.

Changeux, J. P., A. Bessis, et al. (1996). "Nicotinic receptors and brain plasticity." Cold Spring Harb Symp Quant Biol **61**: 343-62.

Court, J., C. Martin-Ruiz, M. Piggot, D. Spurden, M. Griffiths, E. Perry. (2001). "Nicotonic receptor abnormalities in Alzheimer's disease." Biological Psychiatry. **49**: 75-184.

Curtis L., B. B., S. Bertrand, D. Bertrand. (2002). "Potentiation of Human α4β2 Neuronal Nicotinic Acetylcholine Receptor by Estradiol." Molecular Pharmacology. **61**(1): 127-135.

Dani JA, B. D. (2007). "Nicotinic acetylcholine receptors and nicotinic cholinergic mechanisms of the central nervous system." Annu Rev Pharmacol Toxicol **47**: 699-729.

Deneris, E. S., J. Boulter, et al. (1989). "Genes encoding neuronal nicotinic acetylcholine receptors." Clin Chem **35**(5): 731-7.

Elliott, K. J., S. B. Ellis, et al. (1996). "Comparative structure of human neuronal alpha 2-alpha 7 and beta 2-beta 4 nicotinic acetylcholine receptor subunits and functional expression of the alpha 2, alpha 3, alpha 4, alpha 7, beta 2, and beta 4 subunits." Journal Of Molecular Neuroscience: MN **7**(3): 217-28.

Fenster, C. P., M.F. Rains, B. Noerager, M.W. Quick, R.A. Lester. (1997). " Influence of subunit composition on desensitization of neuronal acetylcholine receptors at low concentrations of nicotine." Journal of Neuroscience. **17**(15): 5747-5759.

Frazier, C. J., Y. D. Rollins, et al. (1998). "Acetylcholine activates an alpha-bungarotoxin-sensitive nicotinic current in rat hippocampal interneurons, but not pyramidal cells." J Neurosci **18**(4): 1187-95.

Gay, E. A. and J. L. Yakel (2007). "Gating of nicotinic ACh receptors; new insights into structural transitions triggered by agonist binding that induce channel opening." J Physiol **584**(3): 727-733.

Giniatullin, R., A. Nistri, et al. (2005). "Desensitization of nicotinic ACh receptors: shaping cholinergic signaling." Trends Neurosci **28**(7): 371-8.

Gotti, C. and F. Clementi (2004). "Neuronal nicotinic receptors: from structure to pathology." Prog Neurobiol **74**(6): 363-96.

Gotti, C., D. Fornasari, et al. (1997). "Human neuronal nicotinic receptors." Prog Neurobiol **53**(2): 199-237.

Gotti, C., M. Zoli, et al. (2006). "Brain nicotinic acetylcholine receptors: native subtypes and their relevance." Trends in Pharmacological Sciences **27**(9): 482-491.

Jensen, A. A., B. Frolund, et al. (2005). "Neuronal nicotinic acetylcholine receptors: structural revelations, target identifications, and therapeutic inspirations." J Med Chem **48**(15): 4705-45.

Ji, D., J.A. Dani (2000). "Inhibition and disinhibition of pyramidal neurons by activation of nicotinic receptors on hippocampal interneurons." Journal of Neurophysiology. **83**: 2682-2690.

Jones, S., S. Sudweeks, et al. (1999). "Nicotinic receptors in the brain: correlating physiology with function." Trends Neurosci **22**(12): 555-61.

Jones, S. and J. L. Yakel (1997). "Functional nicotinic ACh receptors on interneurones in the rat hippocampus." J Physiol (Lond) **504**(Pt 3): 603-10.

Khiroug, S. S., P. C. Harkness, et al. (2002). "Rat nicotinic ACh receptor alpha7 and beta2 subunits co-assemble to form functional heteromeric nicotinic receptor channels." The Journal Of Physiology **540**(Pt 2): 425-34.

Laviolette, S. R. and D. van der Kooy (2004). "The neurobiology of nicotine addiction: bridging the gap from molecules to behaviour." Nat Rev Neurosci **5**(1): 55-65.

Levin, E. D. (2002). "Nicotinic receptor subtypes and cognitive function." J Neurobiol **53**(4): 633-40.

Livak, K. J. and T. D. Schmittgen (2001). "Analysis of relative gene expression data using real-time quantitative PCR and the 2(-Delta Delta C(T)) Method." Methods **25**(4): 402-8.

Lopez-Hernandez, G. Y., J. Sanchez-Padilla, et al. (2004). "Nicotine-induced up-regulation and desensitization of alpha 4 beta 2 neuronal nicotinic receptors depend on subunit ratio." Journal of Biological Chemistry **279**(36): 38007-38015.

Luetje, C. W. and J. Patrick (1991). "Both alpha and beta subunits Contribute to the Agonist Sensitivity of
Neuronal Nicotinic Acetylcholine Receptors." The Journal of Neuroscience, **11**(3): 837-845.

McQuiston, A. R. and D. V. Madison (1999). "Nicotinic receptor activation excites distinct subtypes of interneurons in the rat hippocampus." J Neurosci **19**(8): 2887-96.

Miyazawa, A., Y. Fujiyoshi, et al. (2003). "Structure and gating mechanism of the acetylcholine receptor pore." Nature **423**(6943): 949-55.

Moroni, M., R. Zwart, et al. (2006). "alpha 4 beta 2 nicotinic receptors with high and low acetylcholine sensitivity: Pharmacology, stoichiometry, and sensitivity to long-term exposure to nicotine." Molecular Pharmacology **70**(2): 755-768.

Nelson, M. E., A. Kuryatov, et al. (2003). "Alternate stoichiometries of alpha 4 beta 2 nicotinic acetylcholine receptors." Molecular Pharmacology **63**(2): 332-341.

Newhouse, P. A., A. Potter, et al. (1997). "Nicotinic system involvement in Alzheimer's and Parkinson's diseases. Implications for therapeutics." Drugs Aging **11**(3): 206-28.

Ortells, M. O., GG Lunt (1995). "Evolutionary history of the ligand-gated ion-channel superfamily of receptors." Trends Neurosci. **18**: 121-127.

Paterson, D. and A. Nordberg (2000). "Neuronal nicotinic receptors in the human brain." Prog. Neurobiol. **61**: 75-111.

Pettit, D. L., Z. Shao, et al. (2001). "beta-Amyloid(1-42) peptide directly modulates nicotinic receptors in the rat hippocampal slice." J Neurosci **21**(1): RC120.

Pimlott, S., M. Piggott, J. Owens, E. Greally, J Court, E. Jaros, R. Perry, E. Perry, and D. Wyper. (2004). "Nicotinic Acetylcholine Receptor Distribution in Alzheimer 's Disease, Dementia with Lewy Bodies, Parkinson's Disease, and Vascular Dementia: In Vitro Binding Study Using 5-[I25]-A-85380." jNeuropsychopharmacology **209**: 108-116.

Sher, E., Y. Chen, et al. (2004). "Physiological roles of neuronal nicotinic receptor subtypes: new insights on the nicotinic modulation of neurotransmitter release, synaptic transmission and plasticity." Curr Top Med Chem **4**(3): 283-97.

Sudweeks, S. N. and J. L. Yakel (2000). "Functional and molecular characterization of neuronal nicotinic ACh receptors in rat CA1 hippocampal neurons." J Physiol **527 Pt 3**: 515-28.

Swanson, L. W. (1998). Brain Maps: Structure of the Rat Brain. Amsterdam, Elsevier.

Vibat, C. R., J.A. Lasalde, M.G. McNamee, E.L. Ochoa (1995). "Differential desensitization properties of rat neuronal nicotinic acetylcholine receptor subunit combinations expressed in Xenopus laevis oocytes." Cell Molecular Neurobiology **15**(4): 411-425.

Wada, E., K. Wada, et al. (1989). "Distribution of alpha 2, alpha 3, alpha 4, and beta 2 neuronal nicotinic receptor subunit mRNAs in the central nervous system: a hybridization histochemical study in the rat." J Comp Neurol **284**(2): 314-35.

Woodruff-Pak DS, G. T. (2002). "Neuronal nicotinic acetylcholine receptors: involvement in Alzheimer's disease and schizophrenia." Behav Cogn Neurosci Rev **1(1)**: 5-20.

Yu, C. R. and L. W. Role (1998). "Functional contribution of the alpha5 subunit to neuronal nicotinic channels expressed by chick sympathetic ganglion neurones." J Physiol (Lond) **509**(Pt 3): 667-81.

Zwart, R. and H. P. M. Vijverberg (1998). "Four pharmacologically distinct subtypes of alpha 4 beta 2 nicotinic acetylcholine receptor expressed in Xenopus laevis oocytes." Molecular Pharmacology **54**(6): 1124-1131.

John Mizukawa

671 E 500 N Provo, UT 84606
Phone: (801) 368-0351
jhm37@email.byu.edu

Education

- B.S.- Zoology, Brigham Young University, Provo, UT.
August 2005
- M.S.- Physiology and Developmental Biology, Brigham Young University, Provo, UT.
August 2008

Honors and Awards

- BYU Heritage Scholarship recipient - May 2002
- BYU Graduate Student Scholarship recipient –August 2005
- Society for Neuroscience poster presenter 2006 and 2007
- BYU Graduate Student Research Presentation Award recipient 2007

Research Experience

- Undergraduate mentored research with Dr. David Busath MD, 2003-2005, Brigham
Young University, Provo, UT
> Production and identification of synthetic lipid bilayer rafts consisting of DOPC,
> sphingomyelin, and cholesterol using atomic force microscopy.

- Graduate mentored research with Dr. Sterling Sudweeks PhD, 2005-2008, Brigham
Young University, Provo, UT
> Characterization of alpha3 beta2 neuronal nicotinic acetylcholine receptors in rat
> CA1 hippocampal interneurons using patch clamp electrophysiology.

- Guest researcher with Dr. Jerrel Yakel PhD, March 2008, Laboratory of Neurobiology,
NIEHS/NIH, RTP, NC.
> Characterization of alpha3 beta2 neuronal nicotinic acetylcholine receptors in
> *Xenopus laevis* oocytes using voltage-clamp electrophysiology.

Teaching Experience

- Lecturer and lab teaching assistant for advanced physiology lab, BYU 2005-present.
- Two time presenter at Department of Physiology and Developmental Biology Seminar,
BYU 2005 and 2006.

Posters/Presentations

Sterling N. Sudweeks, John Mizukawa, and Kasey Welch. Characterization of alpha3beta2 neuronal nicotinic acetylcholine receptors. Presented at the Annual Meeting of the Society for Neuroscience. Program No. 574.3. November 6, 2007. 2007 Neuroscience Meeting Planner. San Diego, CA: Society for Neuroscience, 2007. Online.

Sudweeks, S.; Mizukawa, J.; Welch, K.; Gay, E.; Yakel, J. Neuronal nicotinic acetylcholine receptor diversity in rat hippocampal interneurons. Presented at the XIII International Symposium on Cholinergic Mechanisms, Foz do Iguaçu – Brazil, August 16-20, 2008.

Sudweeks, S.; Mizukawa, J.; Welch, K.; Gay, E.; Yakel, J. Characterization of neuronal nicotinic acetylcholine receptors in rat hippocampus. To be presented at the Annual Meeting of the Society for Neuroscience. Washington D.C. November 17, 2008.

References

- Dr. Sterling Sudweeks PhD, BYU Associate Professor of Physiology & Developmental Biology, 595 WIDB Provo, UT 84602. (801) 422-8752. sns34@byu.edu
- Dr. James Porter PhD, BYU Department Chair of Physiology and Developmental Biology, 575 WIDB Provo, UT 84602. (801) 422-9160. james_porter@byu.edu
- Dr. Scott Steffensen PhD, BYU Associate Professor of Psychology, 1050 SWKT Provo, UT 84602. (801) 422-9499. scott_steffensen@byu.edu